AD_____

Award Number:
W81XWH-08-1-0117

TITLE:
Novel Optical Methods for Identification, Imaging, and Preservation of the Cavernous Nerves Responsible for Penile Erections during Prostate Cancer Surgery

PRINCIPAL INVESTIGATOR:
Nathaniel M. Fried, Ph.D.

CONTRACTING ORGANIZATION:
University of North Carolina at Charlotte
Charlotte, NC 28223-0001

REPORT DATE:
March 2009

TYPE OF REPORT:
Annual

PREPARED FOR: U.S. Army Medical Research and Materiel Command
Fort Detrick, Maryland 21702-5012

DISTRIBUTION STATEMENT:

X Approved for public release; distribution unlimited

REPORT DOCUMENTATION PAGE

Form Approved
OMB No. 0704-0188

1. REPORT DATE *(DD-MM-YYYY)*	2. REPORT TYPE	3. DATES COVERED *(From - To)*
31-03-2009	Annual	1 Mar 2008 – 28 Feb 2009

4. TITLE AND SUBTITLE
Novel Optical Methods for Identification, Imaging, and Preservation of the Cavernous Nerves Responsible for Penile Erections During Prostate Cancer Surgery

5a. CONTRACT NUMBER
PC073709

5b. GRANT NUMBER
W81XWH-08-1-0117

5c. PROGRAM ELEMENT NUMBER

6. AUTHOR(S)
Nathaniel M. Fried, Ph.D.

5d. PROJECT NUMBER

5e. TASK NUMBER

5f. WORK UNIT NUMBER

7. PERFORMING ORGANIZATION NAME(S) AND ADDRESS(ES)
University of North Carolina at Charlotte
Sponsored Programs
Financial Management
Charlotte, NC 28223-0001

8. PERFORMING ORGANIZATION REPORT NUMBER

9. SPONSORING / MONITORING AGENCY NAME(S) AND ADDRESS(ES)
U.S. Army Medical Research
and Materiel Command
Fort Detrick, MD 21702-5012

10. SPONSOR/MONITOR'S ACRONYM(S)

11. SPONSOR/MONITOR'S REPORT NUMBER(S)

12. DISTRIBUTION / AVAILABILITY STATEMENT
Approved for public release (distribution unlimited)

13. SUPPLEMENTARY NOTES

14. ABSTRACT
There is wide variability in sexual potency rates (9-86%) after prostate cancer surgery due to our limited understanding of the location of the cavernous nerves, which are responsible for erectile function. Advances in identification and preservation of these nerves would result in improved postoperative potency and patient quality of life. We hypothesize that application of three optical technologies for identification, imaging, and preservation of the nerves during prostate surgery will result in improved sexual function: (1) Laser nerve stimulation for identification, optical coherence tomography (OCT) for nerve imaging, and (3) precise laser prostate dissection for nerve preservation. Year 1 was devoted to optimization of laser stimulation parameters and comparison with electrical stimulation. We completed these tasks and then started on Year 2 aims, including assembly of a laparoscopic laser nerve stimulation probe, and improving OCT image quality for differentiating nerves and prostate. We have published our results (2 manuscripts, 5 conference proceedings, and 3 abstracts).

15. SUBJECT TERMS
Laser Nerve Stimulation; Optical Coherence Tomography; Cavernous Nerves

16. SECURITY CLASSIFICATION OF:			17. LIMITATION OF ABSTRACT	18. NUMBER OF PAGES	19a. NAME OF RESPONSIBLE PERSON
a. REPORT	b. ABSTRACT	c. THIS PAGE			USAMRMC
U	U	U	UU	52	19b. TELEPHONE NUMBER *(include area code)*

TABLE OF CONTENTS

INTRODUCTION

One of the greatest challenges of prostate cancer surgery is preservation of sexual function after surgery. There has been a wide variability in reported post-operative potency rates, ranging from 9 – 86%. This variability may be due, in part, to our limited understanding of the location, extent, and course of the cavernous nerves, which are responsible for erectile function. Because of the close proximity of the nerves to the surface of the prostate, they are at risk of damage during surgical dissection and removal of a cancerous prostate. In addition, their microscopic nature makes it difficult to predict the true course and location of these nerves from one individual patient to another. Improvements in identification, imaging, and visualization of these nerves will likely improve the consistency of nerve preservation and postoperative potency and thus lead to an improved quality of life for patients. We hypothesize that the application of novel optical technologies for identification, imaging, and preservation of the cavernous nerves during prostate cancer surgery will result in improved sexual function. We intend to test three optical technologies: Non-contact laser stimulation for identification of the cavernous nerves, high-resolution imaging of the cavernous nerves using optical coherence tomography, and rapid, precise, and hemostatic dissection of the prostate from the cavernous nerves using a KTP laser. Year 1 was devoted to optimization of the laser nerve stimulation parameters and direct comparison with conventional electrical nerve stimulation. We completed these tasks ahead of schedule, and therefore started work on some of the Year 2 aims as well, such as assembly of a laparoscopic laser nerve stimulation probe, and improving the image quality of optical coherence tomography for differentiating the cavernous nerves from the prostate gland. Overall, we published our results in both scientific and clinical journals in the form of 2 manuscripts, 5 conference proceedings, and 3 abstracts. Our research results were also presented at several national and international conferences, including the International Symposium for Biomedical Optics (SPIE), the IEEE Engineering in Medicine and Biology Society (EMBS) annual meeting, the Engineering and Urology Society (EUS) annual meeting, and the Sexual Medicine Society of North America Fall meeting.

BODY

STATEMENT OF WORK (Year 1)

TASK #1. Non-contact laser stimulation of the cavernous nerves (Months 1-18)

A. Optimize laser nerve stimulation parameters (Months 1-6).

***Objective*:** Optimize the laser parameters (wavelength, pulse energy, and pulse rate) to produce strongest and most rapid erectile response as measured by intracavernosal pressure in the penis.

***Criteria for Success*:** Improve the ICP intensity response over baseline (SNR) from 2:1 during preliminary experiments to a ratio of 4:1, and decrease ICP response time during laser stimulation.

***Status*:** Completed.

***Results*:** After optimization of the laser nerve stimulation parameters, we achieved a peak ICP response of approximately 50-60 mmHg. By comparison, during preliminary studies before optimization, the ICP response was only 30-40 mmHg, only 2 times that of the 10-15 mmHg baseline level. Thus, by optimizing the laser stimulation parameters, we have improved the signal-noise ratio from 2:1 to 4:1, meeting our criteria for success, as stated above. Figure 1 shows the strong ICP signal response during laser stimulation, representative of the data collected during our in vivo rat studies in the laboratory.

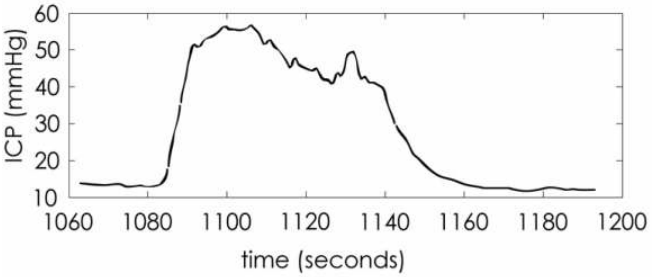

Figure 1. Laser stimulation of the cavernous nerve in the rat prostate.

The optimal laser stimulation parameters were observed at wavelengths of 1860 - 1870 nm, pulse energies of greater than 2.7 - 8 mJ (0.35 - 1.0 J/cm^2), and a pulse rate of 10 Hz. Lower pulse energies and pulse rates failed to produce an ICP response during 60 s stimulation, while higher pulse energies and pulse rates resulted in thermal damage to the nerve and loss of nerve function.

B. Perform direct comparison between electrical and optical nerve (Months 7-12).

***Objective*:** Perform direct comparison between non-contact laser stimulation of cavernous nerves and conventional contact electrical stimulation.

***Criteria for Success*:** Produce at least an equivalent signal (ICP) to noise (baseline) level for laser stimulation as for electrical stimulation.

***Status*:** Completed.

***Results*:** Below are three graphs: electrical nerve stimulation (pre-control), laser nerve stimulation, and electrical nerve stimulation again (post-control) for stimulation of the cavernous nerve on the same rat. Notice that laser nerve stimulation is safe, as evidenced by no significant loss in nerve function upon re-stimulation. Also, notice that laser nerve stimulation is capable of producing not just a comparable ICP response to electrical stimulation, but that laser nerve stimulation may also produce a greater ICP response than electrical nerve stimulation.

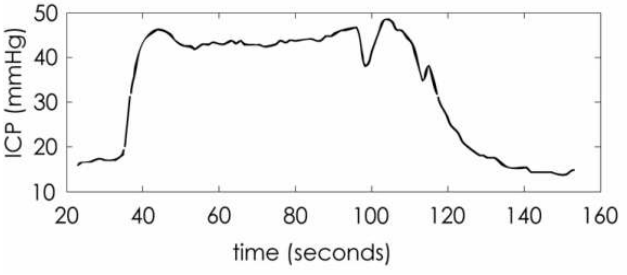

(a) Electrical nerve stimulation (pre-control)

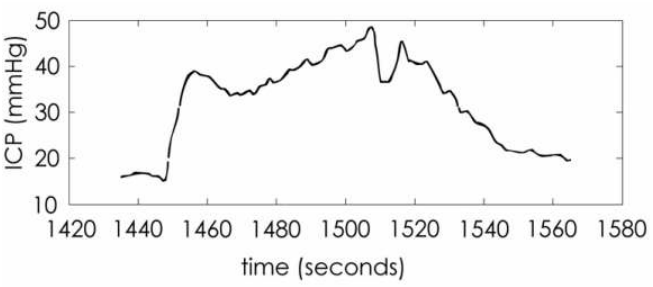

(c) Electrical nerve stimulation (post-control)

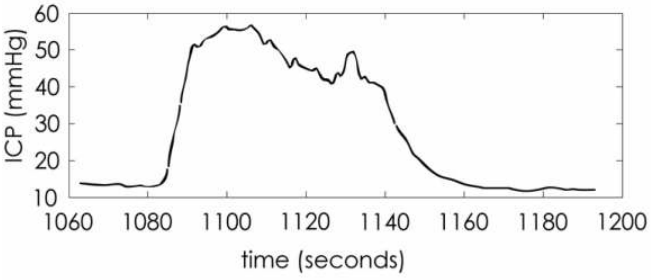

(b) Laser nerve stimulation

Figure 2. Intracavernosal pressure (ICP) response as a function of time for electrical and optical nerve stimulation over a period of 60 s. (a) Electrical stimulation at beginning of study; (b) Laser stimulation; (c) Electrical stimulation at end of study. A comparable ICP response is observed during electrical and laser stimulation, without evidence of loss in ICP signal or nerve function after repeated laser stimulation measurements.

Statement of Work (First half of Year 2)

A. Develop rapid scanning laser nerve stimulation system for prostate surgery (Months 13-18).

***Objective*:** Develop a laparoscopic laser nerve stimulation probe capable of rapid scanning of tissue and identification of the cavernous nerves during prostate cancer surgery.

***Criteria for Success*:** Develop a laparoscopic laser stimulation probe with rapid scanning capability, and with a 4-mm-OD for insertion through a 5-mm-ID laparoscopic port during prostate surgery.

***Status*:** Completed.

***Results*:** A compact laparoscopic probe was designed for future clinical use in optical nerve stimulation. The 10-Fr (3.4-mm-OD) prototype laparoscopic probe includes an aspheric lens for collimation of the laser beam with a 0.8-mm-diameter spot, coupled with a 200-μm-core optical fiber. A 45^{o} gold-coated rod mirror in the probe tip provides side-firing delivery of the laser radiation. The probe handle houses a miniature linear motorized stage for lateral scanning of the probe tip over a

25-mm line along the prostate surface. A 5.5-W Thulium fiber laser with tunable wavelength range of 1850-1880 nm was tested with the probe. The probe fits through a standard 5-mm-ID laparoscopic port and is capable of delivering pulse energies up to 8 mJ (1.6 J/cm^2) at a 2.5-ms pulse duration, well above threshold (~ 0.35 J/cm^2) for optical stimulation of the cavernous nerves (Figure 4).

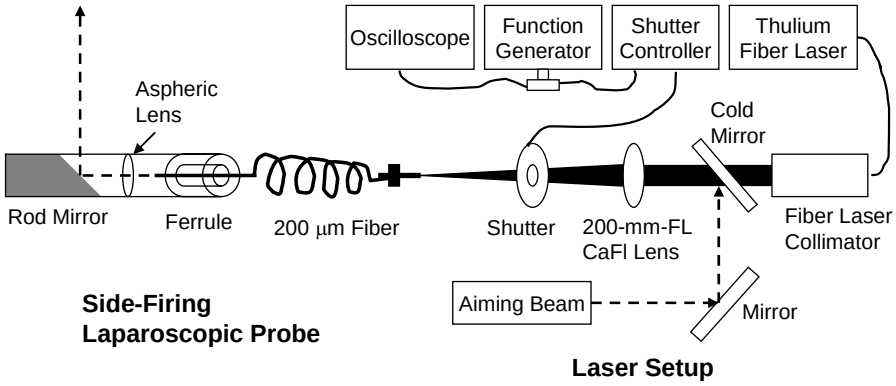

Figure 3. Diagram of experimental setup with fiber optic assembly for laser probe (left) & laser equipment (right).

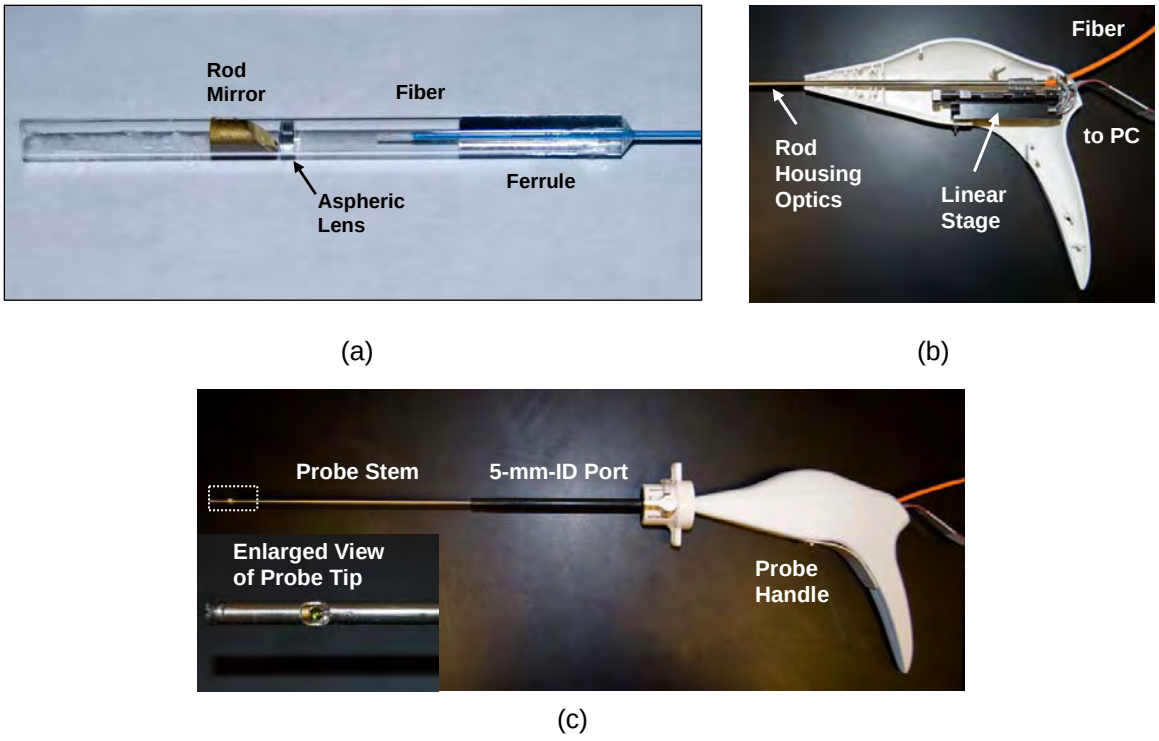

Figure 4. Probe design: (a) Optical component assembly; (b) Linear stage inside probe handle; (c) Assembled probe.

TASK #2. High-resolution imaging of cavernous nerves using Optical Coherence Tomography.

A. Improve OCT image quality (Months 13-18).

Objective: To improve the image quality of optical coherence tomographic images, so the cavernous nerves can be differentiated from the prostate gland with improved depth and resolution.

***Status*:** In progress.

Results: The dual-tree complex wavelet transform (CDWT) is a relatively recent enhancement to the discrete wavelet transform (DWT), with important additional properties. It is nearly shift-invariant and directionally selective in two and higher dimensions. A locally adaptive denoising algorithm is applied to reduce speckle noise in optical coherence tomography images of the prostate. The cavernous nerve and prostate gland can be separated from discontinuities due to noise, and image quality metrics improvements with a signal-to-noise (SNR) ratio increase of 14 dB are attained. Figure 5 shows the OCT images of the nerve and prostate both before and after denoising.

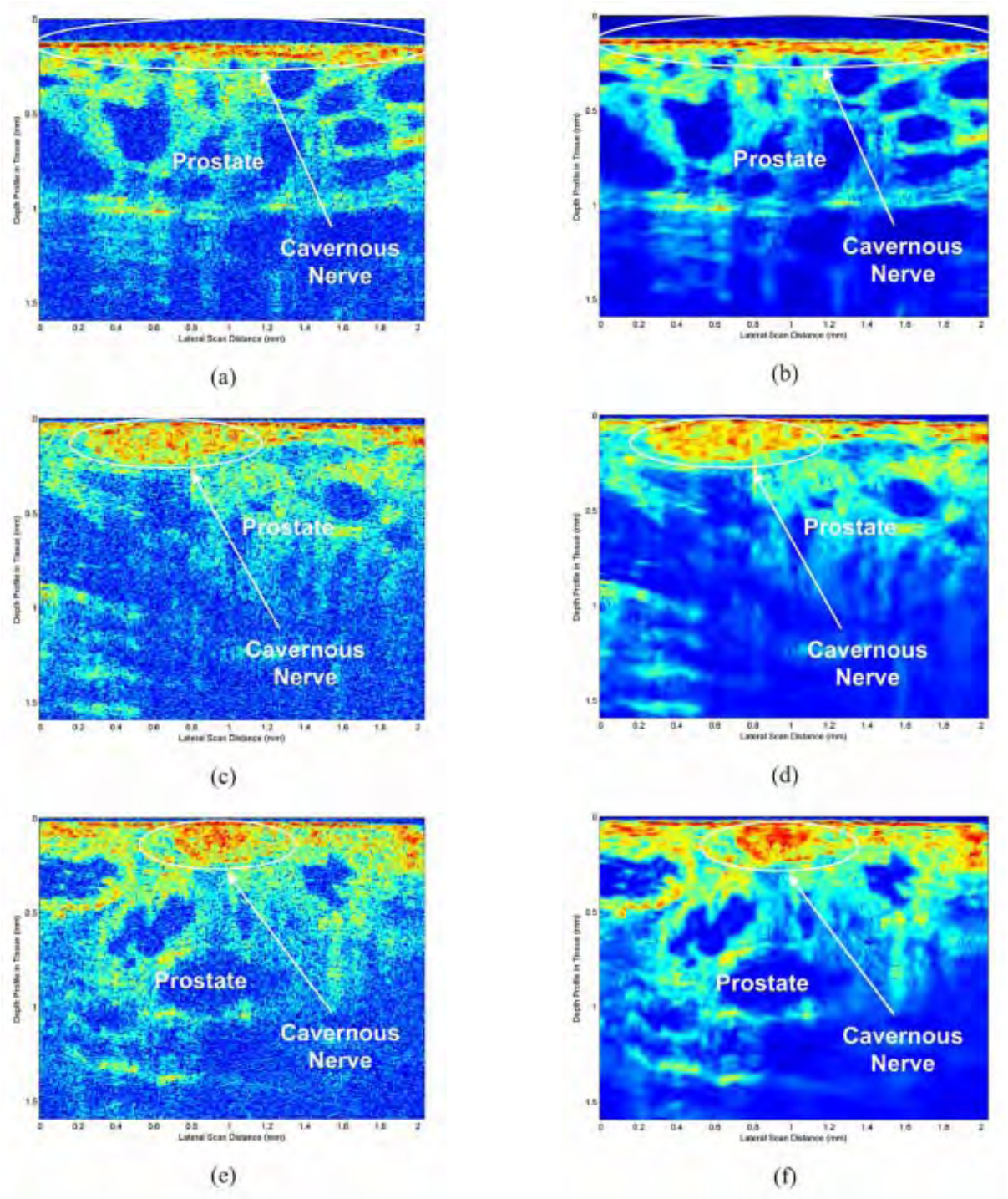

Figure 5. Comparison between original (a,c,e) optical coherence tomography (OCT) images of the cavernous nerves on the rat prostate with denoised (b,d,f) OCT images using our dual-tree complex wavelet transform. A signal-to-noise (SNR) increase of 14 dB was achieved with this algorithm. Each row shows a different orientation of the cavernous nerve: (a,b) longitudinal; (c,d) oblique; and (e,f) cross-sectional.

KEY RESEARCH ACCOMPLISHMENTS

- We optimized the laser parameters (wavelength, pulse energy, and pulse rate) to produce the strongest and most rapid erectile response as measured by intracavernosal pressure (ICP) in the penis. ICP values were increased from an initial range of 30-40 mmHg during preliminary studies to a range of 50-60 mmHg. The optimal laser stimulation parameters were observed at wavelengths of 1860-1870 nm, pulse energies of 2.7–8.0 mJ (0.35-1.0 J/cm^2), and a pulse rate of 10 Hz. Lower pulse energies and pulse rates failed to produce an ICP response during 60 s stimulation, while higher pulse energies and pulse rates resulted in thermal damage to the nerve and loss of nerve function.

- Direct comparative studies between laser nerve stimulation and conventional electrical nerve stimulation were performed, demonstrating no significant difference in peak intracavernosal pressure between the two techniques.

- A compact, laparoscopic laser nerve stimulation probe was designed for use in preclinical and clinical studies. The handheld, side-firing probe is capable of rapid scanning of a laser beam across the surface of the prostate with a laser power density sufficient for nerve stimulation. The probe fits through a standard, 5-mm-OD laparoscopic port typically used in the clinic for laparoscopic and robotic prostate cancer surgery.

- Computer image processing algorithms were applied to optical coherence tomographic images of the rat cavernous nerves and the prostate to de-noise the images and make it easier for a clinician to differentiate between the cavernous nerves and the prostate during prostate cancer surgery. A signal-to-noise (SNR) increase of 14 dB was achieved using these algorithms.

REPORTABLE OUTCOMES

Peer-Reviewed Manuscripts

Rais-Bahrami S, Levinson AW, Fried NM, Lagoda GA, Hristov A, Chuang Y, Burnett AL, Su LM. Optical coherence tomography of cavernous nerves: a step toward real-time intraoperative imaging during nerve-sparing radical prostatectomy. Urology 72(1):198-204, 2008.

Chitchian S, Fiddy MA, Fried NM. Denoising during optical coherence tomography of the prostate nerves via wavelet shrinkage using dual-tree complex wavelet transform. Journal of Biomedical Optics 14(1):014031, 2009.

Peer-Reviewed Conference Proceedings

Fried NM, Lagoda GA, Scott NJ, Su LM, Burnett AL. Laser stimulation of the cavernous nerves in the rat prostate, in vivo: optimization of wavelength, pulse energy, and pulse repetition rate. Conf Proc IEEE Eng Med Biol Soc 1:2777-2780 (Vancouver, BC, 2008).

Chitchian S, Fiddy M, Fried NM. Wavelet denoising during optical coherence tomography of the prostate nerves using the complex wavelet transform. Conf Proc IEEE Eng Med Biol Soc 1:3016-3019 (Vancouver, BC, 2008).

Tozburun S, Fried NM. Design of a compact laparoscopic probe for optical stimulation of the cavernous nerves. Proc. SPIE 7161:716113 (San Jose, CA, 2009).

Chitchian S, Fiddy M, Fried NM. Speckle reduction during all-fiber common-path optical coherence tomography of the cavernous nerves. Proc. SPIE 7168:71682N (San Jose, CA, 2009).

Chitchian S, Fiddy M, Fried NM. Denoising during optical coherence tomography of the prostate nerves via bivariate shrinkage using dual-tree complex wavelet transform. Proc. SPIE 716112 (San Jose, CA, 2009).

Abstracts

Fried NM, Lagoda GA, Su LM, Burnett AL. Noncontact optical stimulation of the cavernous nerves in the rat prostate: optimization of the laser parameters. Journal of Endourology 22(11):2605-2606, 2008.

Chitchian S, Fiddy M, Fried NM. Image processing algorithms for use in optical coherence tomography of the cavernous nerves in the prostate. Journal of Endourology 22(11):2604-2605, 2008.

Lagoda G, Fried N, Burnett A. Optical stimulation of the rat cavernous nerves. Journal of Sexual Medicine 6(s1):8, 2009.

CONCLUSION

In the first year of this project, we accomplished several aims. First, we optimized the laser parameters (wavelength, pulse energy, and pulse rate) to produce the strongest and most rapid erectile response as measured by intracavernosal pressure (ICP) in the penis. After optimization of the laser nerve stimulation parameters, we achieved a peak ICP response of approximately 50-60 mmHg. By comparison, during preliminary studies before optimization, the ICP response was only 30-40 mmHg, only 2 times that of the 10-15 mmHg baseline level. Thus, by optimizing the laser stimulation parameters, we have improved the signal-noise ratio from 2:1 to 4:1. Second, we performed direct comparative studies between laser nerve stimulation and conventional electrical nerve stimulation, and demonstrated no significant difference in peak intracavernosal pressure between the two techniques. Third, a laparoscopic laser nerve stimulation probe was designed for potential use in preclinical and clinical studies. Finally, computer image processing algorithms were applied to optical coherence tomography images of the rat cavernous nerves and the prostate to de-noise the images and make it easier for a clinician to differentiate between the cavernous nerves and the prostate gland during prostate cancer surgery. Overall, we published our results in both scientific and clinical journals in the form of 2 manuscripts, 5 conference proceedings, and 3 abstracts. Our research results were also presented at several national and international conferences, including the International Symposium for Biomedical Optics (SPIE), the IEEE Engineering in Medicine and Biology Society (EMBS) annual meeting, the Engineering and Urology Society (EUS) annual meeting, and the Sexual Medicine Society of North America Fall meeting.

REFERENCES

1. G. P. Murphy, C. Mettlin, H. Menck, D. P. Winchester, and A. M. Davidson, "National patterns of prostate cancer treatment by radical prostatectomy: results of a survey by the American College of Surgeons Committee on Cancer," *J. Urol.*, vol. 152, 1817-1819, 1994.
2. J. A. Talcott, P. Rieker, K. J. Propert, J. A. Clark, K. I. Wishnow, K. R. Loughlin, J. P. Richie, and P. W. Kantoff, "Patient-reported impotence and incontinence after nerve-sparing radical prostatectomy," *J. Natl. Cancer Inst.*, vol. 89, pp. 1117-1123, 1997.
3. V. E. Weldon, F. R. Tavel, and H. Neuwirth, Continence, potency and morbidity after radical perineal prostatectomy," *J. Urol.*, vol. 158:1470-1475, 1997.
4. W. J. Catalona, G. F. Carvalhal, D. E. Mager, and D. S. Smith, "Potency, continence and complication rates in 1,870 consecutive radical retropubic prostatectomies," *J. Urol.*, vol. 162, pp. 433-438, 1999.
5. P. C. Walsh, P. Marschke, D. Ricker, and A. L. Burnett, "Patient-reported urinary continence and sexual function after anatomic radical prostatectomy," *Urol.*, vol. 55, pp. 58-61, 2000.
6. A. L. Burnett, G. Aus, E. D. Canby-Hagino, M. S. Cookson, A. V. D'Amico, R. R. Dmochowski, D. T. Eton, J. D. Forman, S. L. Goldenberg, J. Hernandez, C. S. Higano, S. Kraus, M. Liebert, J. W. Moul, C. Tangen, J. B. Thrasher, I. Thompson, "Erectile function outcome reporting after clinically localized prostate cancer treatment," *J. Urol.*, vol. 178(2), pp. 597-601, 2007.
7. A. J. Costello, M. Brooks, and O. J. Cole, "Anatomical studies of the neurovascular bundle and cavernosal nerves," *BJU Int.*, vol. 94, pp. 1071-1076, 2004.
8. N. M. Fried, S. Rais-Bahrami, G. A. Lagoda, Y. Chuang, A. L. Burnett, and L. M. Su, "Imaging the cavernous nerves in the rat prostate using optical coherence tomography," *Lasers Surg. Med.*, vol. 39, pp. 36-41, 2007.
9. D. Huang, E. A. Swanson, C. P. Lin, J. S. Schuman, W. G. Stinson, W. Chang, M. R. Hee, T. Flotte, K. Gregory, C. A. Puliafito, and J. G. Fujimoto, "Optical coherence tomography," *Science*, vol. 254, pp. 1178-1181, 1991.
10. G. J. Tearney, M. E. Brezinski, B. E. Bouma, S. A. Boppart, C. Pitris, J. F. Southern, and J. G. Fujimoto, "In vivo endoscopic optical biopsy with optical coherence tomography," *Science*, vol. 276, pp. 2037-2039, 1997.
11. F. Koenig, G. J. Tearney, and B. E. Bouma, "Optical coherence tomography in urology," Ch. 28, In Handbook of Optical Coherence Tomography, Eds. B. E. Bouma and G. J. Tearney, Marcel Dekker: New York, 2002.
12. P. Crow, N. Stone, C. A. Kendall, R. A. Persad, and M. P. Wright, "Optical diagnostics in urology: current applications and future prospects," *BJU Int.*, vol. 92, pp. 400-407, 2003.
13. G. J. Tearney, M. E. Brezinski, J. F. Southern, B. E. Bouma, S. A. Boppart, and J. G. Fujimoto, "Optical biopsy in human urologic tissue using optical coherence tomography," *J. Urol.*, vol. 157, pp. 1915-1919, 1997.
14. A. V. D'Amico, M. Weinstein, X. Li, J. P. Richie, and J. Fujimoto, "Optical coherence tomography as a method for identifying benign and malignant microscopic structures in the prostate gland," *Urol.*, vol. 55, pp. 783-787, 2000.
15. S. A. Boppart, J. M. Herrmann, C. Pitris, D. L. Stamper, M. E. Brezinski, and J. G. Fujimoto, "Real-time optical coherence tomography for minimally invasive imaging of prostate ablation," *Comput. Aided Surg.*, vol. 6, pp. 94-103, 2001.
16. L. Klotz, "Neurostimulation during radical prostatectomy: improving nerve-sparing techniques," *Semin. Urol. Oncol.*, vol. 18, pp. 46-50, 2000.
17. H. L. Kim, D. S. Stoffel, D. A. Mhoon, and C. B. Brendler, "A positive caver map response poorly predicts recovery of potency after radical prostatectomy," *Urol.*, vol. 56, pp. 561-564, 2000.
18. L. Klotz, J. Heaton, M. Jewett, J. Chin, N. Fleshner, L. Goldenberg, and M. Gleave, "A randomized phase 3 study of intraoperative cavernous nerve stimulation with penile

tumescence monitoring to improve nerve sparing during radical prostatectomy," *J. Urol.*, vol. 164, pp. 1573-1578, 2000.
19. J. Holzbeierlein, M. Peterson, and J. A. Smith Jr, "Variability of results of cavernous nerve stimulation during radical prostatectomy," *J. Urol.*, vol. 165, pp. 108-110, 2001.
20. P. C. Walsh, P. Marschke, W. J. Catalona, H. Lepor, S. Martin, R. P. Myers, and M. S. Steiner, "Efficacy of first-generation Cavermap to verify location and function of cavernous nerves during radical prostatectomy: a multi-institutional study by experienced surgeons," *Urol.*, vol. 57, pp. 491-494, 2001.
21. H. L. Kim, D. A. Mhoon, and C. B. Brendler, "Does the CaverMap device help preserve potency?" *Curr. Urol. Rep.*, vol. 2, pp. 214-217, 2001.
22. L. Klotz, "Cavernosal nerve mapping: current data and applications," *BJU Int.*, vol. 93, pp. 9-13, 2004.
23. J. Wells, C. Kao, K. Mariappan, J. Albea, E. D. Jansen, P. Konrad, and A. Mahadevan-Jansen, "Optical stimulation of neural tissue in vivo," *Opt. Lett.*, vol. 30, pp. 504-506, 2005.
24. J. Wells, C. Kao, E. D. Jansen, P. Konrad, and A. Mahadevan-Jansen, "Application of infrared light for in vivo neural stimulation," *J. Biomed. Opt.*, vol. 10:064003, pp. 1-11, 2005.
25. A. D. Izzo, C. P. Richter, E. D. Jansen, and J. T. Walsh, "Laser stimulation of the auditory nerve," *Lasers Surg. Med.*, vol. 38, pp. 745-753, 2006.
26. A. D. Izzo, J. T. Walsh, E. D. Jansen, M. Bendett, J. Webb, H. Ralph, and C. P. Richter, "Optical parameter variability in laser nerve stimulation: a study of pulse duration, repetition rate, and wavelength," *IEEE Trans. Biomed. Eng.*, vol. 54, pp. 1108-1114, 2007.
27. J. D. Wells, S. Thomsen S, P. Whitaker, E. D. Jansen, C. C. Kao, P. E. Konrad, A. Mahadevan-Jansen, "Optical mediated nerve stimulation: identification of injury thresholds," *Lasers Surg. Med.* vol. 39, pp. 513-526, 2007.
28. J. Bush, P. Davis, and M. A. Marcus, "All-fiber optic coherence domain interferometric techniques," *Proc. SPIE*, vol. 4204A-08, 2000.
29. F. Feldchtein, J. Bush J, G. Gelikonov, V. Gelikonov, and S. Piyevsky S, "Cost-effective, all-fiber autocorrelator based 1300 nm OCT system," *Proc. SPIE*, vol. 5690, pp. 349-354, 2005.
30. U. Sharma, N. M. Fried, and J. U. Kang, "All-fiber common-path optical coherence tomography: sensitivity optimization and system analysis," *IEEE J. Sel. Top. Quant. Electron.*, vol. 11, pp. 799-805, 2005.
31. F. Feldchtein, N. Tresser, M. Kareta, D. Bodner, I. Gill, J. Kaouk, P. Kick, G. MacLennan, W. Kuang, L. Schoenfeld, E. Klein, M. Resnick, "Niris optical coherence tomography system: principle of operation and applications in endourology," *J. Endourol.*, vol. 20 (Suppl 1):A198, 2006.
32. M. Aron, J. H. Kaouk, N. J. Hegarty, J. R. Colombo, Jr., G. P. Haber, B. I. Chung, M. Zhou, I. S. Gill, "Preliminary experience with the Niris optical coherence tomography system during laparoscopic and robotic prostatectomy," *J. Endourol.*, vol. 21(8), pp. 814-818, 2007.

APPENDIX

Peer-Reviewed Manuscripts

Rais-Bahrami S, Levinson AW, Fried NM, Lagoda GA, Hristov A, Chuang Y, Burnett AL, Su LM. Optical coherence tomography of cavernous nerves: a step toward real-time intraoperative imaging during nerve-sparing radical prostatectomy. Urology 72(1):198-204, 2008.

Chitchian S, Fiddy MA, Fried NM. Denoising during optical coherence tomography of the prostate nerves via wavelet shrinkage using dual-tree complex wavelet transform. Journal of Biomedical Optics 14(1):014031, 2009.

Peer-Reviewed Conference Proceedings

Fried NM, Lagoda GA, Scott NJ, Su LM, Burnett AL. Laser stimulation of the cavernous nerves in the rat prostate, in vivo: optimization of wavelength, pulse energy, and pulse repetition rate. Conf Proc IEEE Eng Med Biol Soc 1:2777-2780 (Vancouver, BC, 2008).

Chitchian S, Fiddy M, Fried NM. Wavelet denoising during optical coherence tomography of the prostate nerves using the complex wavelet transform. Conf Proc IEEE Eng Med Biol Soc 1:3016-3019 (Vancouver, BC, 2008).

Tozburun S, Fried NM. Design of a compact laparoscopic probe for optical stimulation of the cavernous nerves. Proc. SPIE 7161:716113 (San Jose, CA, 2009).

Chitchian S, Fiddy M, Fried NM. Speckle reduction during all-fiber common-path optical coherence tomography of the cavernous nerves. Proc. SPIE 7168:71682N (San Jose, CA, 2009).

Chitchian S, Fiddy M, Fried NM. Denoising during optical coherence tomography of the prostate nerves via bivariate shrinkage using dual-tree complex wavelet transform. Proc. SPIE 716112 (San Jose, CA, 2009).

Abstracts

Fried NM, Lagoda GA, Su LM, Burnett AL. Noncontact optical stimulation of the cavernous nerves in the rat prostate: optimization of the laser parameters. Journal of Endourology 22(11):2605-2606, 2008.

Chitchian S, Fiddy M, Fried NM. Image processing algorithms for use in optical coherence tomography of the cavernous nerves in the prostate. Journal of Endourology 22(11):2604-2605, 2008.

Lagoda G, Fried N, Burnett A. Optical stimulation of the rat cavernous nerves. Journal of Sexual Medicine 6(s1):8, 2009.

Optical Coherence Tomography of Cavernous Nerves: A Step Toward Real-Time Intraoperative Imaging During Nerve-Sparing Radical Prostatectomy

Soroush Rais-Bahrami, Adam W. Levinson, Nathaniel M. Fried, Gwen A. Lagoda, Alexandra Hristov, Ying Chuang, Arthur L. Burnett, and Li-Ming Su

OBJECTIVES To demonstrate the use of optical coherence tomography (OCT) for imaging of the cavernous nerve (CN) and periprostatic tissues. The rates of nerve preservation and postoperative potency after radical prostatectomy might improve with better identification of the CN using emerging intraoperative imaging modalities. OCT is an imaging modality that allows for real-time, high-resolution, cross-sectional imaging of tissues.

METHODS Seven male Sprague-Dawley rats underwent surgery using a midline celiotomy to expose the bladder, prostate, and seminal vesicles. The CNs and major pelvic ganglion were identified. Visual identification of the CN was further confirmed by electrical stimulation with simultaneous intracorporeal pressure measurements. OCT images of the CN, major pelvic ganglion, bladder, prostate, and seminal vesicles were acquired and correlated directly with the histologic findings. Once a baseline technique for the scanning and interpretation of the acquired images was established using the rat model, OCT was used to image ex vivo human prostatectomy specimens.

RESULTS OCT provided unique imaging characteristics, differentiating the CN from the bladder, prostate, seminal vesicles, and periprostatic fat. OCT images of the CN and prostate correlated well with the histologic findings. OCT of ex vivo human prostatectomy specimens revealed findings similar to those with the rat experiments, with, however, less dramatic architecture visualized in part because of the thicker capsule and more dense stroma of human prostates.

CONCLUSIONS The results of our study have shown that OCT provides real-time, high-resolution imaging of the CN in the rat model with excellent correlation to the histologic findings. This study provides a basis for the intraoperative use of this emerging technology during nerve-sparing prostatectomy. UROLOGY 72: 198–204, 2008. © 2008 Elsevier Inc.

CAVERNOUS NERVE PRESERVATION DURING RADICAL PROSTATECTOMY

The reported rates of postoperative potency after nerve-sparing radical prostatectomy have ranged widely from 21% to 86%.[1–5] Many factors contribute to this wide range of potency, including patient characteristics (preoperative potency, age, presence of sexual partner, and medical comorbidities), oncologic factors (cancer stage and grade), and surgeon skill (technique and experience with nerve-sparing prostatectomy). Recently, reports have been published that have suggested that the variability in the course of the cavernous nerves (CNs) could also contribute to the variation in the rates of postoperative potency.[6–8] Because of the microscopic nature of the CN and its superficial course along the surface of the prostate, it is challenging to clearly visualize the exact course of the nerves in each individual patient to avoid injury during resection of the cancerous prostate gland. The rates of nerve preservation and postoperative potency after radical prostatectomy could improve with better identification of the CN by incorporating real-time intraoperative imaging. To aid in the identification and preservation of the CN, numerous imaging modalities are currently under investigation to assess their possible role in developing a more individualized anatomic CN-sparing radical prostatectomy. In this study, we investigated the use of optical coherence tomography (OCT) for

From the James Buchanan Brady Urological Institute and Department of Pathology, Johns Hopkins Medical Institutions, Bethesda, Maryland; and Department of Physics and Optical Science, University of North Carolina at Charlotte, Charlotte, North Carolina

Reprint requests: Li-Ming Su, M.D., Department of Urology, Division of Laparoscopic and Robotic Surgery, James Buchanan Brady Urological Institute, Johns Hopkins Medical Institutions, Jefferson Street Building, Suite 161, 600 North Wolfe Street, Baltimore, MD 21287. E-mail: lsu11@jhmi.edu

Submitted: August 25, 2007, accepted (with revisions): November 16, 2007

0090-4295/08/$34.00
doi:10.1016/j.urology.2007.11.084

imaging of the CN in the rat model, as well as in ex vivo human prostatectomy specimens.

OPTICAL COHERENCE TOMOGRAPHY

OCT is an emerging imaging modality that allows for real-time, high-resolution, cross-sectional imaging of tissues and is being integrated into multiple medical disciplines. Analogous to B-mode ultrasonography, OCT measures backscatter near-infrared light rather than sound, obtaining images of tissues with resolutions several orders of magnitude greater (1 to 15 μm) than that achieved with ultrasonography.[9,10] Currently, clinical OCT systems are being used in ophthalmology and cardiology. Application of OCT to urologic practice is being actively studied, and the initial reports of OCT imaging of the genitourinary tissues, including the prostate, urethra, ureters, kidneys, and bladder, have been published.[11–17]

Several aspects of OCT make this a very attractive imaging modality for surgical disciplines. The compact, fiberoptic nature delivery system for OCT has allowed it to be integrated into existing surgical instruments, including catheters, hand-held probes, and needles.[18–20] OCT also offers localized, high-resolution imaging of the area of interest and lends itself to portability, unlike radiologic cross-sectional imaging modalities such as computed tomography and magnetic resonance imaging. Finally, the OCT systems are available at a relatively low cost because their components are already mass produced for the telecommunications industry.

The aim of this study was to explore the use of OCT for diagnostic imaging of the CN and periprostatic structures in situ in the rat animal model and in ex vivo prostatectomy specimens, with the eventual goal of implementing this technology into real-time intraoperative mapping of the CN during nerve-sparing radical prostatectomy.

MATERIAL AND METHODS

Niris OCT System

All imaging in this study was performed with the commercially available Niris OCT system (Imalux, Cleveland, Ohio), which acquires real-time images with 200 × 200 pixels and an axial to lateral resolution of 11 to 25-μm to a maximal depth of 1.6 mm. The system consists of a computer console and screen on which the real-time images are seen. A handheld 8F (2.7 mm OD) Niris probe is connected to the console and used for transmission of near-infrared light to the tissues and can be rotated to achieve various angles of cross-section imaging, very similar to ultrasonography. Foot pedal attachment allows for hands-free acquisition and storing of OCT images.

In Vivo Imaging of Rat Periprostatic Structures

The prostate, CN, major pelvic ganglion, bladder, and seminal vesicles were identified by way of midline celiotomy in seven male Sprague-Dawley rats weighing between 400 and 600 g. CN electrical stimulation with simultaneous intracorporeal pressure measurements was performed to provide physiologic confirmation of the CN. Increased intracorporeal pressure and augmented penile length and girth were clearly demonstrated, confirming the location and course of the rat CN. OCT images were then acquired of the CN and periprostatic structures, localizing the CN based on both direct visualization and electrical stimulation (Fig. 1, Video 1-4). Finally, the prostate was removed en bloc and processed for hematoxylin-eosin histologic correlation, as described in detail by Fried *et al.*[21]

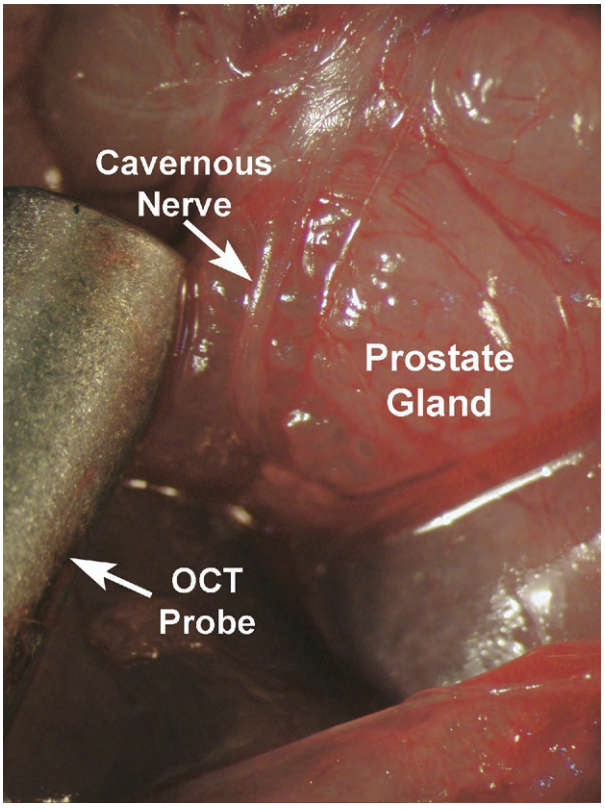

Figure 1. Close-up view of in vivo OCT imaging probe on prostate gland adjacent to CN in rat model.

Ex Vivo Imaging of Human Prostatectomy Specimens

Once a baseline technique for scanning and interpretation of the acquired images was established in the rat model, OCT was used to image ex vivo human prostatectomy specimens. OCT imaging was performed on human prostates in the operating room, immediately after specimen extraction following robot-assisted laparoscopic radical prostatectomy. Five cases of robot-assisted laparoscopic radical prostatectomy were performed by a single surgeon (L.S.) from October 2006 to January 2007 in which unilateral wide excision of the neurovascular bundle (NVB) was required because of concern of local extension of cancer into the NVB. The resected specimens were passed off of the sterile field and the prostate gland, CN, and other associated periprostatic structures were scanned using OCT before submitting the specimen to surgical pathology for final diagnosis and staging (Fig. 2).

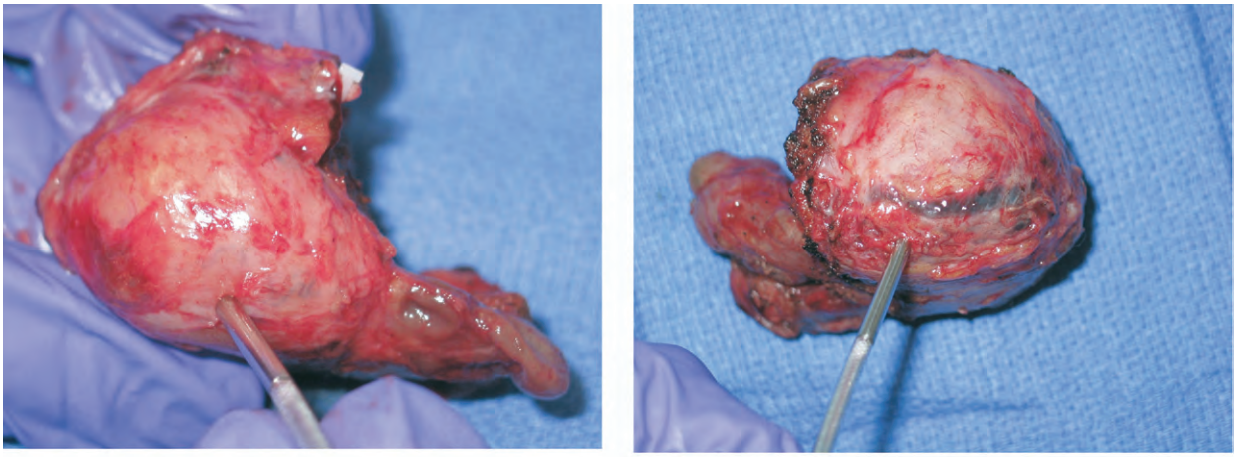

A B

Figure 2. Ex vivo setup for OCT imaging of CN and other periprostatic structures for ex vivo human prostatectomy specimens after robot-assisted laparoscopic radical prostatectomy. **(A)** Robotic-assisted radical prostatectomy specimen with NVB spared. **(B)** Robotic-assisted radical prostatectomy specimen with NVB resected.

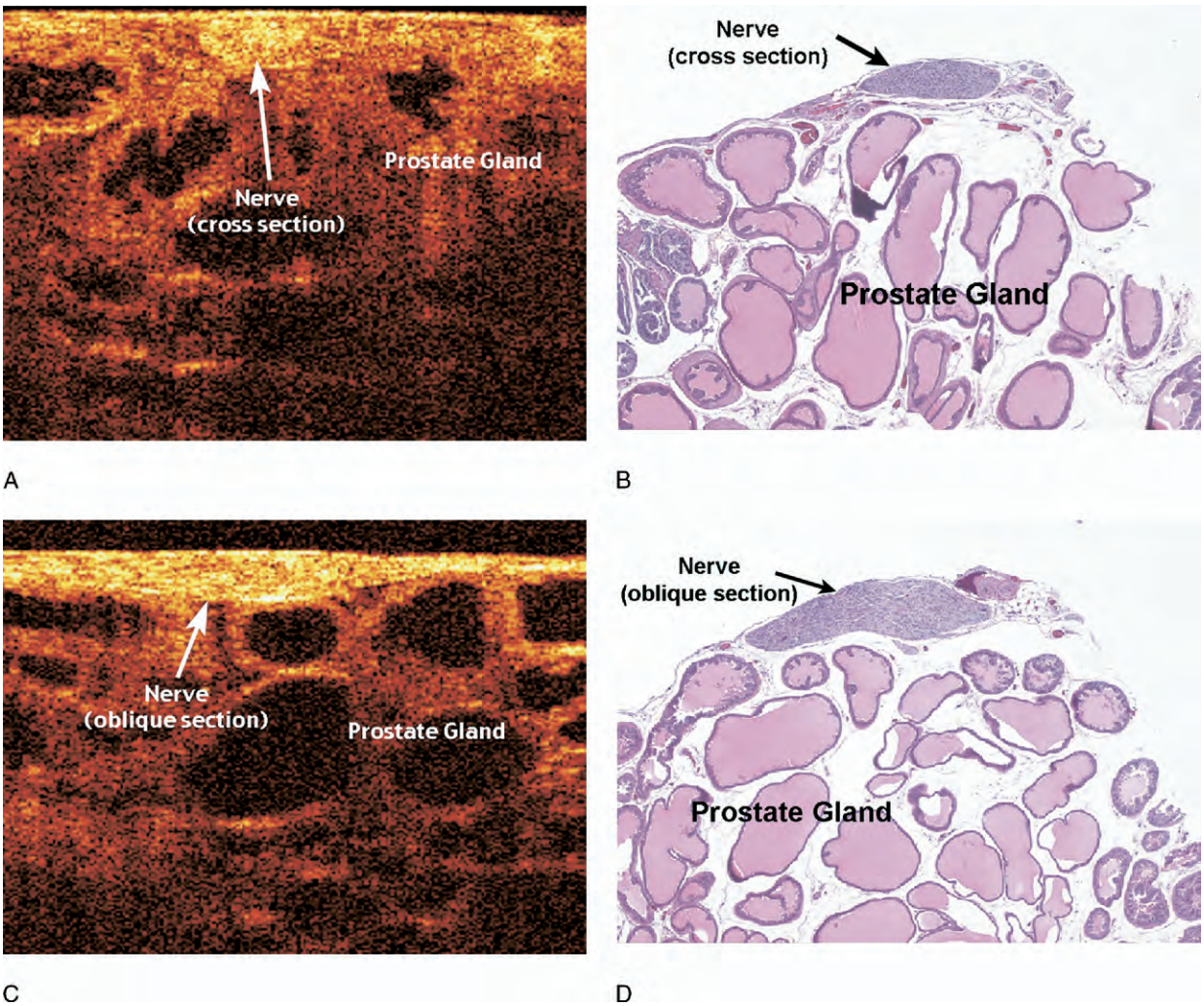

A B C D

Figure 3. OCT imaging and histologic (hematoxylin-eosin) correlation of rat CN **(A,B)** in cross section and **(C,D)** in oblique section overlying prostate glandular tissue.

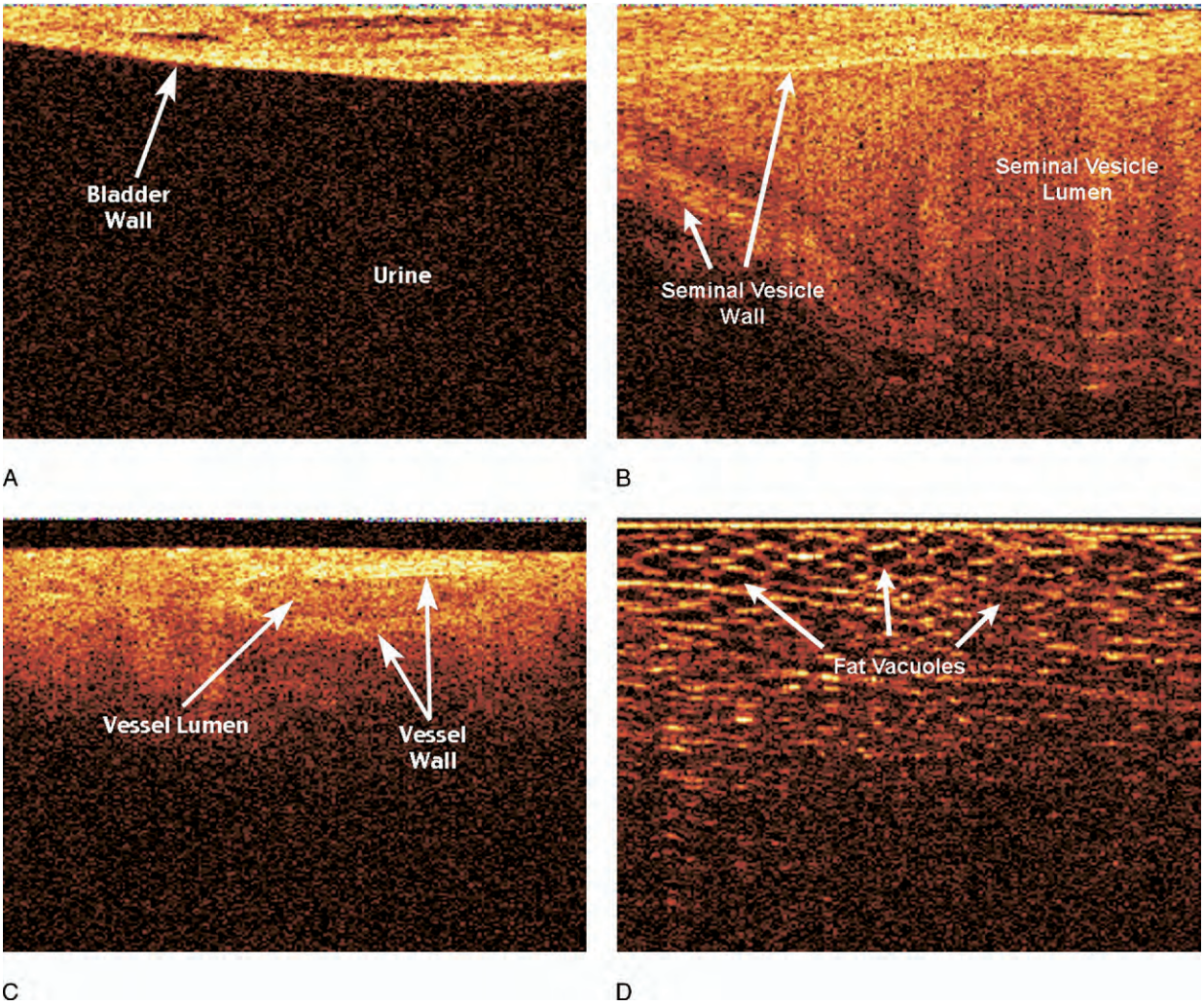

Figure 4. OCT images of rat **(A)** bladder wall, **(B)** seminal vesicle, **(C)** blood vessel, and **(D)** adipose tissue.

RESULTS

In Vivo Imaging of Rat Periprostatic Structures

In our rat experiments, the CN was first identified visually, with physiologic confirmation by electrical stimulation. With this basis, we then applied OCT imaging to evaluate the appearance of the CNs with respect to the surrounding periprostatic tissues, including the prostate gland, bladder, seminal vesicles, blood vessels, and periprostatic fat. We found that OCT provided unique imaging characteristics for each of these tissues, with the longitudinal CN and major pelvic ganglion images appearing as hyperdense, linear structures, likely because of their superficial nature allowing for less signal attenuation and light scatter, as well as the brighter coloration of the nerve tissue allowing for more reflection of light. The prostatic tissue underlying the CN appeared less intense with large vacuolated glands. OCT images of the nerve and underlying prostate glandular architecture correlated extremely well with the representative hematoxylin-eosin histologic sections (Fig. 3). The bladder appeared as a thick-walled structure surrounding a large urine-filled lumen; the seminal vesicles appeared as a thick wall surrounding a less-intense fluid containing lumen, the blood vessels appeared as a medium-intensity rim surrounding a mixed-density fluid-filled lumen, and adipose tissue appeared as a fine lace-like pattern (Fig. 4).

Ex Vivo Imaging of Human Prostatectomy Specimens

The OCT imaging of human prostatectomy specimens revealed findings very similar to those of the rat study, allowing for identification of the CN superficially as a linear, dense signal intensity, which correlated with histologic examination of the same (Fig. 5A-D). OCT imaging clearly identified the CNs and vessels in the NVB and pathologic examinations of the specimens confirmed the presence of the NVB on the side in which the NVB was not spared. In the prostatectomy specimens analyzed, the nerves were only spared unilaterally, providing an internal control within each specimen, for which OCT revealed a paucity of supracapsular vessels and CNs later confirmed with pathologic examination (Fig. 5E,F).

Despite the very similar findings in scanning human CN and prostatic tissue, OCT imaging of human speci-

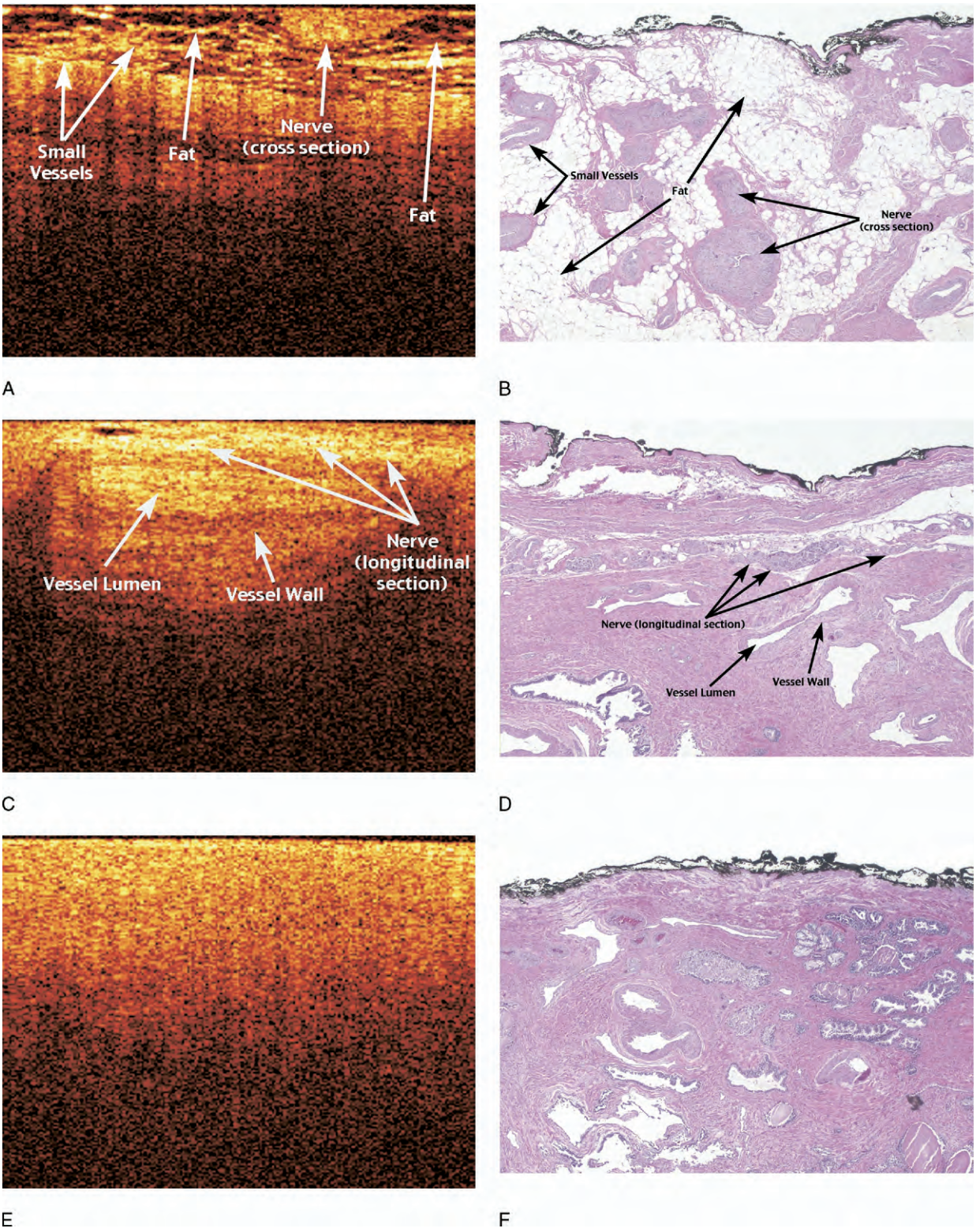

Figure 5. (A-D) OCT imaging and histologic (hematoxylin-eosin) correlation of ex vivo human prostatectomy specimens revealing intact overlying neurovascular bundle. **(E,F)** OCT imaging and histologic (hematoxylin-eosin) correlation of ex vivo human prostatectomy specimens revealing prostate gland without overlying NVB on contralateral nerve-sparing side of resection specimen.

mens was more challenging than in the rat because of the abundance of blood vessels and fat traveling along with the CNs within the NVB. In addition, the relatively greater density of the prostatic capsule and stroma of the human prostate compared with the rat prostate resulted in a significant loss of signal contrast, making discrimi-

nation between the CN and underlying prostate gland more difficult.

COMMENT

Recent anatomic studies investigating the location and course of the CN have raised some questions as to the precise distribution and course of these nerve fibers traveling in the NVB alongside the prostate gland.[6–8] These studies were based on histologic evaluation of human cadavers and suggest that the CNs might have a more diffuse branching than previously thought, and their distribution might be different from one individual to another.[6] This anatomic variability in the CN distribution could in part explain the wide range in potency results found after nerve-sparing radical prostatectomy. Taken together, these findings highlight the importance for additional exploration of imaging modalities that would allow for real-time anatomic mapping of the CNs, allowing for individualized preservation of these nerves during prostatectomy.

During open retropubic radical prostatectomy, surgeons have long used the cavernous vessels as a macroscopic landmark for where the CNs travel within the NVB. Laparoscopy has allowed for improved visualization of the periprostatic structures, but despite the magnification provided, the precise course of the microscopic CNs remains elusive. Ukimura and Gill[22] have proposed the use of real-time transrectal ultrasonography of the NVB to aid in guiding nerve preservation during laparoscopic radical prostatectomy. With this technique, pulsations within the NVB are used to identify the cavernous vessels within the NVB, providing a surrogate for locating the CNs. Although transrectal ultrasonography provides real-time feedback, once again the CNs are not directly visualized but rather assumed to course amidst the visible cavernous vessels.

In the present study, we have reported the successful use of OCT for real-time in situ imaging of the CNs in the rat animal model. The rat model was chosen for this study, because it is a well-known animal model for studying the CN. In the rat, the CN exists as a large, visible structure, with very little surrounding blood vessels and fatty tissue, making it ideal for identification and imaging using OCT. The CNs were visually identified and confirmed physiologically by electrical stimulation, and the OCT images were then correlated with the hematoxylin-eosin histologic findings. We found that OCT correlated well with the histologic findings in differentiating the CN from the underlying prostate glandular architecture. Furthermore, OCT imaging of the periprostatic structures such as the bladder, prostate gland, seminal vesicles, and periprostatic fat, provided a unique imaging signature for each of these structures, allowing for easy interpretation and differentiation between the different tissue types.

Despite OCT's excellent resolution and discrimination of the CN from the surrounding periprostatic tissues in the rat model, it did not provide as consistent a contrast in the human prostatectomy specimens imaged, likely as a consequence of the differing capsular and glandular tissue density. Because this study was performed with a first-generation OCT device, additional improvements in light sources might improve the imaging depth, resolution, and differentiation between minor changes in tissue architecture to better visualize human prostates and periprostatic structures. In addition, further modification of OCT delivery could allow for such technology to be placed at the end of robotic and laparoscopic instruments, allowing for precise mapping of the CNs during radical prostatectomy. Ideally, OCT could be used to image the topographic landscape of the entire posterolateral aspect of the prostate, revealing the course of the CNs and sites of nerve branching otherwise not grossly visible.

CONCLUSIONS

The results of our study have shown that OCT provides excellent real-time, high-resolution imaging of the CN and periprostatic structures in the rat animal model. OCT images correlate well with the representative histologic findings of the CN and underlying prostatic tissue. OCT technology provides great promise as an intraoperative imaging modality for precise and individualized CN preservation during radical prostatectomy.

References

1. Murphy GP, Mettlin C, Menck H, *et al:* National patterns of prostate cancer treatment by radical prostatectomy: results of a survey by the American College of Surgeons Committee on Cancer. J Urol **152:** 1817-1819, 1994.
2. Talcott JA, Rieker P, Propert KJ, *et al:* Patient-reported impotence and incontinence after nerve-sparing radical prostatectomy. J Natl Cancer Inst **89:** 1117-1123, 1997.
3. Weldon VE, Tavel FR, and Neuwirth H: Continence, potency and morbidity after radical perineal prostatectomy. J Urol **158:** 1470-1475, 1997.
4. Catalona WJ, Carvalhal GF, Mager DE, *et al:* Potency, continence and complication rates in 1,870 consecutive radical retropubic prostatectomies. J Urol **162:** 433-438, 1999.
5. Walsh PC, Marschke P, Ricker D, *et al:* Patient-reported urinary continence and sexual function after anatomic radical prostatectomy. Urology **55:** 58-61, 2000.
6. Takenaka A, Murakami G, Soga H, *et al:* Anatomical analysis of the neurovascular bundle supplying penile cavernous tissue to ensure a reliable nerve graft after radical prostatectomy. J Urol **172:** 1032-1035, 2004.
7. Lunacek A, Schwentner C, Fritsch H, *et al:* Anatomical radical retropubic prostatectomy: "curtain dissection" of the neurovascular bundle. BJU Int **95:** 1226-1231, 2005.
8. Costello AJ, Brooks M, and Cole OJ: Anatomical studies of the neurovascular bundle and cavernosal nerves. BJU Int **94:** 1071-1076, 2004.
9. Huang D, Swanson EA, Lin CP, *et al:* Optical coherence tomography. Science **254:** 1178-1181, 1991.
10. Tearney GJ, Brezinski ME, Bouma BE, *et al:* In vivo endoscopic optical biopsy with optical coherence tomography. Science **276:** 2037-2039, 1997.
11. Tearney GJ, Brezinski ME, Southern JF, *et al:* Optical biopsy in human urologic tissue using optical coherence tomography. J Urol **157:** 1915-1919, 1997.

12. Jesser CA, Boppart SA, Pitris C, *et al:* High resolution imaging of transitional cell carcinoma with optical coherence tomography: feasibility for the evaluation of bladder pathology. Br J Radiol **72:** 1170-1176, 1999.
13. D'Amico AV, Weinstein M, Li X, *et al:* Optical coherence tomography as a method for identifying benign and malignant microscopic structures in the prostate gland. Urology **55:** 783-787, 2000.
14. Boppart SA, Herrmann JM, Pitris C, *et al:* Real-time optical coherence tomography for minimally invasive imaging of prostate ablation. Comput Aided Surg **6:** 94-103, 2001.
15. Zagaynova EV, Streltsova OS, Gladkova ND, *et al:* In vivo optical coherence tomography feasibility for bladder disease. J Urol **167:** 1492-1496, 2002.
16. Crow P, Stone N, Kendall CA, *et al:* Optical diagnostics in urology: current applications and future prospects. BJU Int **92:** 400-407, 2003.
17. Manyak MJ, Gladkova ND, Makari JH, *et al:* Evaluation of superficial bladder transitional-cell carcinoma by optical coherence tomography. J Endourol **19:** 570-574, 2005.
18. Tearney GJ, Boppart SA, Bouma BE, *et al:* Scanning single-mode fiber optic catheter-endoscope for optical coherence tomography. Opt Lett **21:** 543-545, 1996.
19. Boppart SA, Bouma BE, Pitris C, *et al:* Forward-imaging instruments for optical coherence tomography. Opt Lett **22:** 1618-1620, 1997.
20. Li X, Chudoba C, Ko T, *et al:* Imaging needle for optical coherence tomography. Opt Lett **25:** 1520-1522, 2000.
21. Fried NM, Rais-Bahrami S, Lagoda GA, *et al:* Imaging the cavernous nerves in the rat prostate using optical coherence tomography. Lasers Surg Med **39:** 36-41, 2007.
22. Ukimura O, and Gill IS: Real-time transrectal ultrasound guidance during nerve sparing laparoscopic radical prostatectomy: pictorial essay. J Urol **175:** 1311-1319, 2006.

Video Clips cited in this article can be found on the internet at: http://www.goldjournal.net

Denoising during optical coherence tomography of the prostate nerves via wavelet shrinkage using dual-tree complex wavelet transform

Shahab Chitchian
Michael A. Fiddy
University of North Carolina at Charlotte
Department of Physics and Optical Science
Charlotte, North Carolina 28223

Nathaniel M. Fried
University of North Carolina at Charlotte
Department of Physics and Optical Science
Charlotte, North Carolina 28223
and
Johns Hopkins Medical Institutions
Department of Urology
Baltimore, Maryland 21287

Abstract. The dual-tree complex wavelet transform (CDWT) is a relatively recent enhancement to the discrete wavelet transform (DWT), with important additional properties. It is nearly shift-invariant and directionally selective in two and higher dimensions. In this letter, a locally adaptive denoising algorithm is applied to reduce speckle noise in time-domain optical coherence tomography (OCT) images of the prostate. The algorithm is illustrated using DWT and CDWT. Applying the CDWT provides improved results for speckle noise reduction in OCT images. The cavernous nerve and prostate gland can be separated from discontinuities due to noise, and image quality metrics improvements with a signal-to-noise ratio increase of 14 dB are attained.
[DOI: 10.1117/1.3081543]

Keywords: wavelet denoising; optical coherence tomography; prostate nerves.

Paper 08350LR received Oct. 1, 2008; revised manuscript received Dec. 9, 2008; accepted for publication Dec. 31, 2008; published online Feb. 19, 2009.

1 Introduction

Optical coherence tomography (OCT) is a noninvasive optical imaging technique used to perform high-resolution cross-sectional *in vivo* and *in situ* imaging of microstructure in biological tissues.[1] OCT imaging of the cavernous nerves in the rat and human prostate has recently been demonstrated.[2–5] However, improvements in the quality of the images for identification of the cavernous nerves during prostate cancer surgery would aid preservation of the nerves and improve postoperative sexual function.

Speckle occurs in the OCT image when the particles composed in the underlying tissue structures are smaller than the coherence length of the light source.[6] Because the speckle pattern is uncorrelated at different positions, angles, and optical wavelengths, speckle reduction using spatial and frequency compounding techniques cannot remove speckle from images acquired with standard OCT systems. Recently, wavelet techniques have been employed successfully in speckle noise reduction for OCT images.[7,8] Wavelet shrinkage denoising is denoising by nonlinear soft thresholding in the wavelet transform domain. Adler et al.[7] applied the discrete wavelet transform (DWT) which provides the most compact representation; however, it has several limitations. The dual-tree complex wavelet transform (CDWT) overcomes these limitations because it is nearly shift-invariant and is oriented in 2-D.[8,9] The complex wavelet transform was used for wavelet denoising in OCT images.[10,11] Forouzanfar et al.[10] applied the directional Bayesian estimator to remove noise from the wavelet coefficients, and we[11] applied a single threshold globally for all relevant parts of the transform in OCT images of experimental systems.

In this study, we have gone one main step further to apply the wavelet shrinkage technique, using CDWT, to an FDA approved clinical endoscopic OCT system. For this purpose, a bivariate shrinkage with local variance estimation algorithm is applied,[12] because the performance of the wavelet shrinkage algorithm for OCT image denoising can be improved by considering the statistical dependencies among wavelet coefficients. We compare the results of the DWT and CDWT algorithms for wavelet shrinkage denoising of *in vivo* OCT images of the rat prostate.

2 Wavelet shrinkage denoising

Denoising attempts to remove noise and retain signal regardless of the frequency content of the signal. Wavelet shrinkage is denoising by shrinking (nonlinear soft thresholding) in the wavelet transform domain.

The observed image, X, is modeled as an uncorrupted image, S, and multiplicative speckle noise, N. On a logarithmic scale, speckle is converted to additive noise, $X=S+N$. The wavelet shrinkage denoising algorithm requires the following four-step procedure,[13]

$$Y = W(X)$$
$$\lambda = d(Y)$$
$$Z = D(Y,\lambda)$$
$$S = W^{-1}(Z) \qquad (1)$$

Address all correspondence to Shahab Chitchian, Dept. of Physics and Optical Science, University of North Carolina at Charlotte, North Carolina 28223. E-mail: schitchi@uncc.edu

1083-3668/2009/14(1)/014031/6/$25.00 © 2009 SPIE

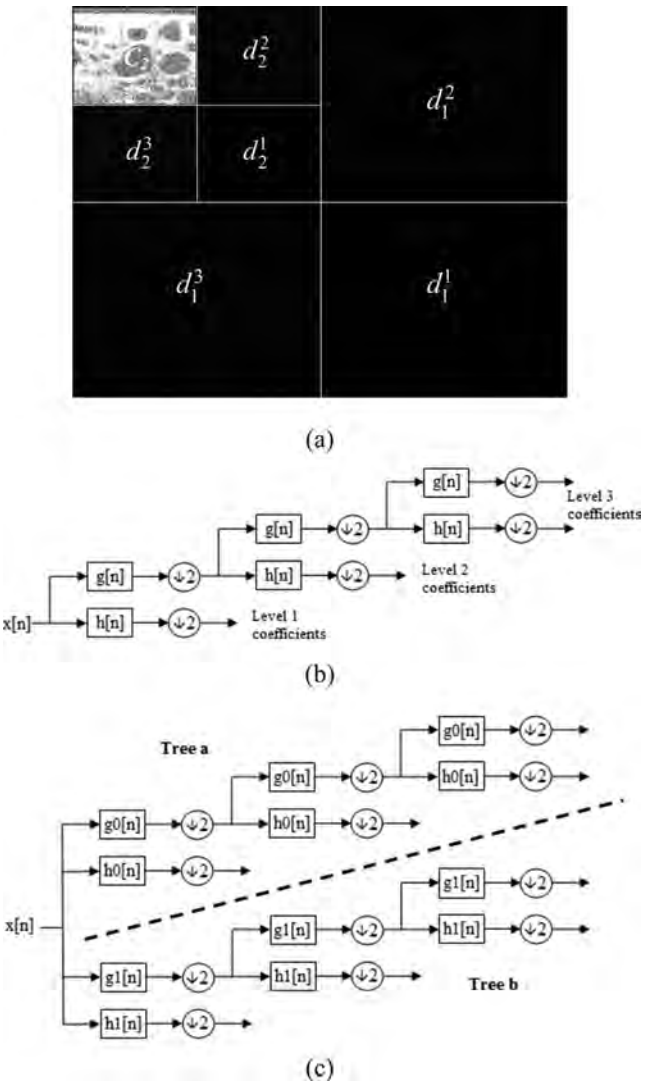

Fig. 1 (a) Ordering of the approximation and detail coefficients of a two-level 2-D DWT; (b) a three-level DWT; (c) a three-level CDWT wavelet filter banks.

3 Wavelet transform

Operator $W(.)$ relates to the wavelet transform, which is the representation of a function by scaled and translated copies of a finite-length or fast-decaying oscillating waveform, which can be used to analyze signals at multiple scales. Wavelet coefficients carry both time and frequency information, as the basis functions vary in position and scale.

3.1 *2-D DWT*

The DWT converts a signal to its wavelet representation. In a one-level DWT, a signal c_0 is split into an approximation part c_1 and a detail part d_1. In a multilevel DWT, each subsequent c_i is split into an approximation c_{i+1} and detail d_{i+1}. For 2-D images, each c_i is split into an approximation c_{i+1} and three detail channels d_{i+1}^1, d_{i+1}^2 and d_{i+1}^3 for horizontally, vertically, and diagonally oriented details, respectively, Figures 1(a) and 1(b). The inverse DWT reconstructs each c_i from c_{i+1} and d_{i+1}.

Table 1 Image quality values.

No.	Image	CNR (dB)	ENL	SNR (dB)
	Original	3.33	1168.6	23.36
1	Denoised (DWT)	4.97	1425.5	26.56
	Denoised (CDWT)	5.63	1490.9	27.13
	Original	9.09	1420.9	27.50
2	Denoised (DWT)	11.44	1824.5	43.47
	Denoised (CDWT)	12.03	1932.4	45.27
	Original	9.11	1276.9	27.99
3	Denoised (DWT)	11.04	1555.7	46.59
	Denoised (CDWT)	11.48	1609.9	46.06
	Original	11.96	1580.4	28.07
4	Denoised (DWT)	13.79	1796.6	35.78
	Denoised (CDWT)	14.08	1866.3	35.64
	Original	7.67	1621.7	26.76
5	Denoised (DWT)	10.79	2255.4	49.84
	Denoised (CDWT)	11.39	2442.9	47.60
	Original	7.05	893.2	28.61
6	Denoised (DWT)	8.40	1043.7	46.95
	Denoised (CDWT)	8.86	1080.6	45.21
	Original	9.50	1974.1	25.62
7	Denoised (DWT)	13.02	2672.1	41.57
	Denoised (CDWT)	13.56	2894.8	43.90
	Original	12.44	3575.3	26.88
8	Denoised (DWT)	18.62	6771.6	43.47
	Denoised (CDWT)	19.32	7580.6	43.42
	Original	4.67	1014.1	25.13
9	Denoised (DWT)	6.23	1202.0	32.91
	Denoised (CDWT)	6.90	1303.0	33.59
	Original	8.31	1613.9	26.65
Mean	Denoised (DWT)	10.92	2283.0	40.79
	Denoised (CDWT)	11.47	2466.8	40.87

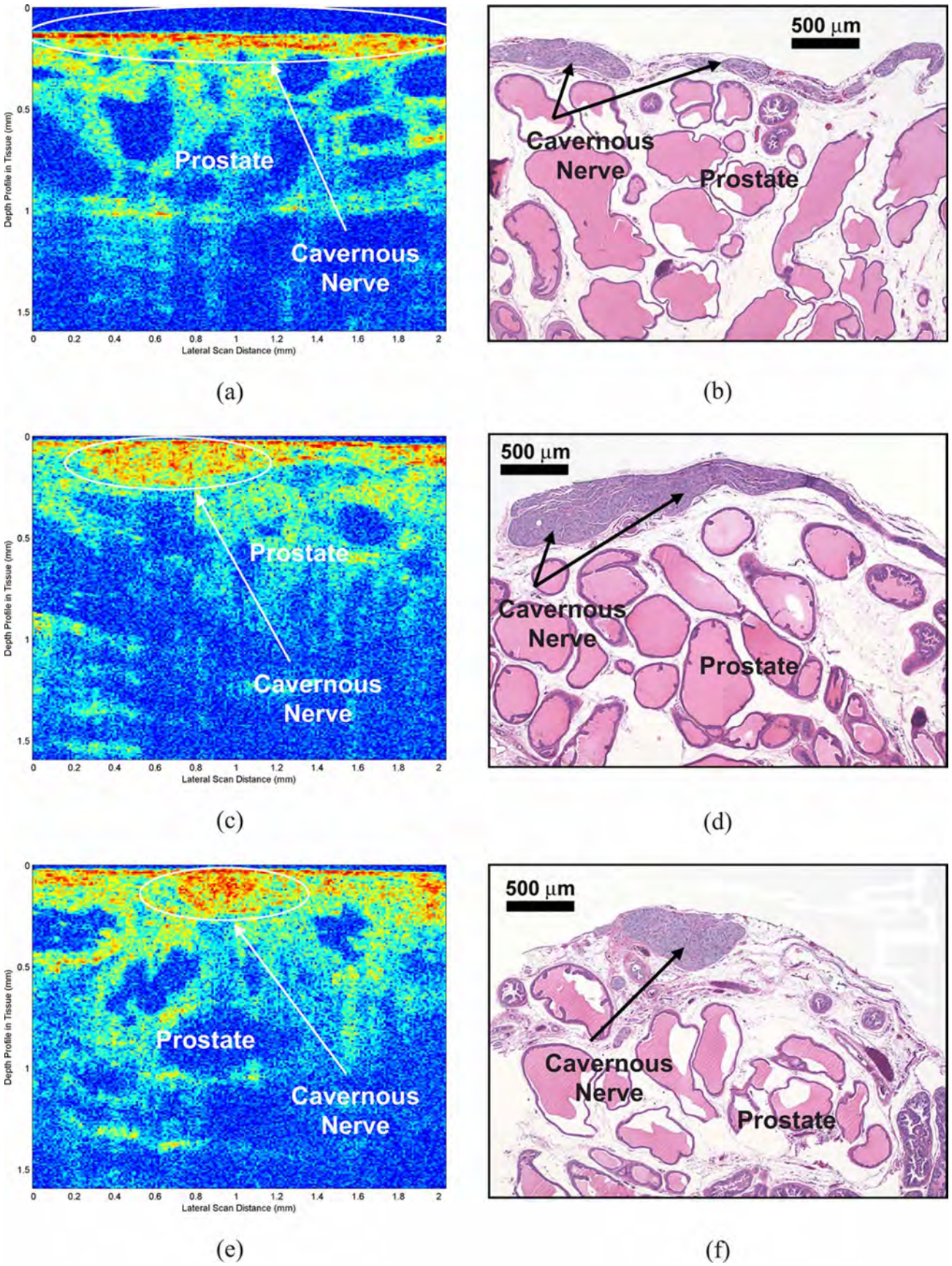

Fig. 2 OCT and corresponding histologic images of the rat cavernous nerve: (a,b) longitudinal section, (c,d) oblique section, and (e,f) cross section. In each section, the cavernous nerve corresponds to a relatively high signal intensity (shown in red) and lies superficial to the prostate. (color online only.)

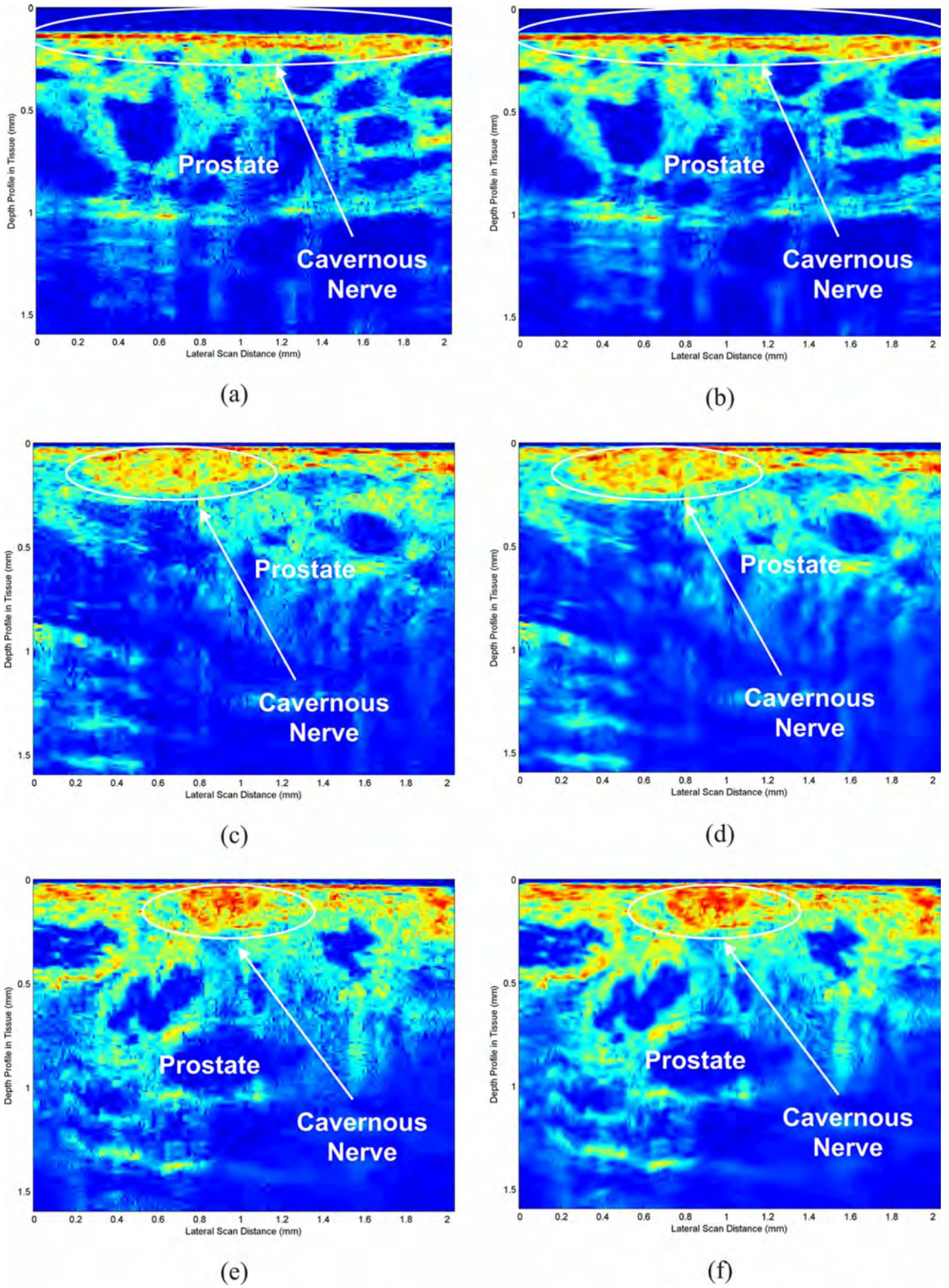

Fig. 3 OCT images of the rat cavernous nerve after wavelet shrinkage denoising: (a,c,e) using DWT and (b,d,f) using CDWT. In comparison to DWT, CDWT has the advantages of being nearly shift-invariant and oriented in two dimensions.

3.2 *2-D CDWT*

The CDWT calculates the complex transform of a signal using two separate DWT decompositions [trees a and b, Fig. 1(c)]. If the filters used in one are specifically designed differently from those in the other, it is possible for one DWT to produce the real coefficients and the other the imaginary coefficients. This redundancy of two provides extra information for analysis but at the expense of extra computational power.

The wavelet transform, W, must be specified by its analysis and synthesis wavelet filter banks. In our case, wavelet coefficients are calculated from the Farras nearly symmetric wavelet.[14] The wavelet transform package by Selesnick et al.[15] was used for implementation of the wavelet transform.

4 Shrinkage denoising

Operator $d(.)$ in Eq. (1) selects a data-adaptive threshold, and $D(.,\lambda)$ denotes the denoising operator with threshold λ. Bivariate shrinkage with local variance estimation algorithm[12] is applied for shrinkage denoising. After estimating the signal components of the noisy coefficients in the wavelet domain, the inverse wavelet transform, W^{-1}, is taken to reconstruct the noise-free image.

5 Results

Figure 2 shows time-domain OCT images of the cavernous nerves at different orientations (longitudinal, oblique, and cross-sectional) coursing along the surface of the rat prostate. OCT images were taken *in vivo* using a clinical endoscopic OCT system (Imalux, Cleveland, OH) which is based on a novel, low-maintenance, low-cost, lightweight OCT system using an all single-mode fiber common-path interferometer-based scanning system (Optiphase, Van Nuys, CA). Histologic sections of the cavernous nerves were processed for comparison, Fig. 2. Figure 3 shows the images after denoising using DWT and CDWT. Image-quality metrics were used to assess performance by measuring the average contrast-to-noise ratio, $\mathrm{CNR}_n = 10 \times \log(\mu_n - \mu_b / \sqrt{\sigma_n^2 + \sigma_b^2})$,[6] and the average equivalent number of looks, $\mathrm{ENL}_n = \mu_n^2 / \sigma_n^2$,[7] over the region of interest which is the location of the cavernous nerve in each image. μ_n is the mean of the pixel values in the location of the cavernous nerve, σ_n is the pixel standard deviation, and μ_b and σ_b are the pixel mean and standard deviation of a background region of the image, respectively. All calculations are made after logarithmic transformation of the image. In addition, the global SNR is calculated as $\mathrm{SNR} = 10 \times \log[\max(X_\mathrm{lin})^2 / \sigma_\mathrm{lin}^2]$, where X_lin is the 2-D matrix of pixel values in the OCT image and σ_lin^2 is the noise variance, both on linear intensity scales.[6]

The values of CNR, ENL and SNR for nine sample images show significant improvement, Table 1. A paired t-test was performed for comparison of original and denoised images, with statistical significance given by values of $P < 0.05$. Comparison of original and CDWT denoised images results in P values for CNR, ENL, and SNR of 0.0003, 0.07, and 0.0001, respectively. The values for CNR and SNR are considered to be statistically significant. Comparison of DWT and CDWT results in P values for CNR, ENL, and SNR of 0.0001, 0.05, and 0.9, respectively. The values for CNR and ENL are considered to be statistically significant.

DWT lacks the shift-invariance property, and in multiple dimensions it performs poorly for distinguishing orientations, which is important in image processing. In other words, this lack of orientation selectivity greatly complicates modeling and processing of geometric image features like the ridges and edges in which the cavernous nerves belong.[16] Therefore, denoising using CDWT, which is more selective with respect to orientation and provides approximate shift-invariance, overcomes this problem and still allows excellent reconstruction of the image. These properties make the CDWT better in denoising than the normal DWT. Comparison of CNR, ENL, and SNR values for DWT and CDWT verifies this; however, we can also visually recognize the advantage of shrinkage denoising using the CDWT.

6 Conclusion

The wavelet shrinkage denoising technique was used for speckle noise reduction in the OCT images of cavernous nerves in the rat prostate. Two different wavelet transform procedures were used, DWT and CDWT, and their denoising results were compared for identification of the cavernous nerves. The CDWT was used to take advantage of this transform, which is shift-invariant and directionally selective. An SNR increase of 14 dB with significant image quality improvements was obtained. This algorithm for wavelet denoising may be a useful technique for clinical OCT applications.

Acknowledgments

This research was supported in part by the Department of Energy, Grant No. DE-FG02-06CH11460, an Idea Development Award from the Department of Defense Prostate Cancer Research Program, Grant No. PC073709, and a Faculty Research Grant from the University of North Carolina at Charlotte. The authors thank Nancy Tresser of Imalux Corporation (Cleveland, OH) for lending us the Niris OCT system for these studies.

References

1. D. Huang, E. Swanson, C. Lin, J. Schuman, W. Stinson, W. Chang, M. Hee, T. Flotte, K. Gregory, C. Puliafito, and J. Fujimoto, "Optical coherence tomography," *Science* **254**, 1178–1181 (1991).
2. M. Aron, J. Kaouk, N. Hegarty, J. Colombo, G. Haber, B. Chung, M. Zhou, and I. Gill, "Preliminary experience with the niris optical coherence tomography system during laparoscopic and robotic prostatectomy," *J. Endourol* **21**, 814–818 (2007).
3. N. Fried, S. Rais-Bahrami, G. Lagoda, A. Chuang, A. Burnett, and L. Su, "Imaging the cavernous nerves in rat prostate using optical coherence tomography," *Lasers Surg. Med.* **39**, 36–41 (2007).
4. N. Fried, S. Rais-Bahrami, G. Lagoda, A. Chuang, L. Su, and A. Burnett, "Identification and imaging of the nerves responsible for erectile function in rat prostate, in vivo, using optical nerve stimulation and optical coherence tomography," *IEEE J. Sel. Top. Quantum Electron.* **13**, 1641–1645 (2007).
5. S. Rais-Bahrami, A. Levinson, N. Fried, G. Lagoda, A. Hristov, A. Chuang, A. Burnett, and L. Su, "Optical coherence tomography of cavernous nerves: A step toward real-time intraoperative imaging during nerve-sparing radical prostatectomy," *Urology* **72**, 198–204 (2008).
6. S. Xiang, L. Zhou, and J. Schmitt, "Speckle noise reduction for optical coherence tomography," *Proc. SPIE* **3196**, 79−88 (1997).
7. D. Adler, T. Ko, and J. Fujimoto, "Speckle reduction in optical coherence tomography images by use of a spatially adaptive wavelet filter," *Opt. Lett.* **29**, 2878–2880 (2004).

8. A. Pizurica, L. Jovanov, B. Huysmans, V. Zlokolica, P. Keyser, F. Dhaenens, and W. Philips, "Multiresolution denoising for optical coherence tomography: A review and evaluation," *Curr. Med. Imaging Rev.* **2008**, 270–284.
9. N. Kingsbury, "Complex wavelets for shift invariant analysis and filtering of signals," *Appl. Comput. Harmon. Anal.* **10**, 234–253 (2002).
10. M. Forouzanfar and H. Moghaddam, "A directional multiscale approach for speckle reduction in optical coherence tomography images," in *Proc. IEEE Electrical Engineering*, p. 1 (2007).
11. S. Chitchian, M. Fiddy, and N. Fried, "Wavelet denoising during optical coherence tomography of the prostate nerves using the complex wavelet transform," in *Proc. of IEEE Engineering in Medicine and Biology*, p. 3016 (2008).
12. L. Sendur and I. Selesnick, "Bivariate shrinkage with local variance estimation," *IEEE Signal Process. Lett.* **9**, 438–441 (2002).
13. C. Taswell, "The what, how, and why of wavelet shrinkage denoising," *Rep. Sci. Res. Inst.* **2**, 12–19 (2000).
14. A. Abdelnour and I. Selesnick, "Design of 2-band orthogonal near-symmetric CQF," in *Proc. IEEE Int. Conf. Acoust., Speech, Signal Processing*, p. 3693 (2001).
15. I. Selesnick, S. Cai, K. Li, L. Sendur, and A. Abdelnour, "Matlab implementation of wavelet transforms," ⟨http://taco.poly.edu/WaveletSoftware/⟩.
16. I. Selesnick, R. Baraniuk, and N. Kingsbury, "The dual-tree complex wavelet transform," *IEEE Signal Process. Mag.* **2005**, 123–151.

Laser Stimulation of the Cavernous Nerves in the Rat Prostate, In Vivo: Optimization of Wavelength, Pulse Energy, and Pulse Repetition Rate

Nathaniel M. Fried, Gwen A. Lagoda, Nicholas J. Scott, Li-Ming Su, and Arthur L. Burnett

***Abstract* – The cavernous nerves on the prostate surface are responsible for erectile function. Improved diagnostic techniques are necessary for identification of the nerves during prostate cancer surgery and preservation of sexual function after surgery. Electrical mapping of the nerves has been used as an intra-operative tool during prostate surgery, but it has proven inconsistent and unreliable. Non-contact optical stimulation of the cavernous nerves in the rat prostate has recently been demonstrated as a potential alternative to electrical nerve stimulation. The purpose of this study is to optimize the laser parameters to provide the maximum intracavernosal pressure response after optical nerve stimulation in the rat prostate. Optimal laser nerve stimulation parameters provided comparable response to electrical nerve stimulation. Optical nerve stimulation may represent a potential intra-operative diagnostic technique for use in laparoscopic and robotic nerve-sparing prostate cancer surgery.**

I. INTRODUCTION AND BACKGROUND

A. Cavernous Nerves

Preservation of the cavernous nerves (CN) during prostate cancer surgery is critical in preserving a man's ability to have spontaneous erections following surgery. Because of the close proximity of the nerves to the prostate surface, they are at risk of injury during dissection and removal of a cancerous prostate gland. Their microscopic nature also makes it difficult to predict the location and path of these nerves from one patient to another. These observations may explain the wide variability in reported sexual potency rates (21-86%) following prostate cancer surgery [1-6]. Recent anatomic studies also suggest that the CN may have more extensive branching along the prostate surface than originally thought, and that our current understanding of the location, extent, and course of these nerves may be limited [7]. Improvements in identification of the CN during surgery would aid preservation of the nerves and improve post-operative potency, resulting in direct patient benefit.

Several optical diagnostic technologies have recently been studied for improved identification of the CN, including optical coherence tomography (OCT) [8-11] and fluorescence imaging [12,13]. Our laboratory has also demonstrated the feasibility of using near-infrared laser radiation for non-contact optical stimulation of the CN in a rat model [10,14]. The rat prostate serves as an excellent model for studying the CN, as the rat cavernous nerve is a large, visible, and distinct bundle allowing for easy identification.

B. Nerve Stimulation

Conventional electrical stimulation of the CN is used in scientific studies to measure erectile response. Intraoperative nerve mapping devices have also been used as a surgical diagnostic tool to assist in preservation of the CN during nerve-sparing prostate cancer surgery [15-21]. However, these nerve mapping technologies have proven inconsistent and unreliable in both identifying the CN and evaluating nerve function.

Electrical nerve stimulation in general has several limitations. First, it is limited by the need for physical contact between the electrode and the tissue, which may result in tissue damage. Second, the spatial precision of stimulation is limited by the electrode's size. Third, electrical stimulation itself produces artifacts that may interfere with measurement.

Recently, optical stimulation of nerves has been demonstrated using pulsed infrared lasers [22-26]. Laser nerve stimulation offers several advantages over electrical stimulation including: (1) a non-contact method of stimulation, (2) improved spatial selectivity, and (3) elimination of stimulation artifacts.

The purpose of this study is to optimize the laser parameters (wavelength, pulse energy, and pulse repetition rate), for optical stimulation of the cavernous nerve in the rat prostate. The optimal laser stimulation parameters would provide the highest magnitude intracavernosal pressure (ICP) response over a short duration.

II. MATERIALS AND METHODS

A. Animal Surgical Preparation

Ten male Sprague Dawley rats weighing approximately 300 grams were anesthetized by intraperitoneal injection with 50 mg/kg sodium pentobarbital. The rats were secured in the supine position and prepped for surgery. The CN arising from the ipsilateral major pelvic ganglion situated dorsolateral to the prostate was exposed via a midline suprapubic incision and anterior pelvic dissection.

This research was supported in part by an Idea Development Award from the Department of Defense Prostate Cancer Research Program, Grant #PC073709, and a Wachovia New Faculty Summer Research Grant from the Charlotte Research Institute.

N. M. Fried and Nicholas J. Scott are with the Department of Physics and Optical Science at the University of North Carolina at Charlotte, Charlotte, NC 28223 USA (phone: 704-687-8149; fax: 704-687-8197; e-mail: nmfried@uncc.edu).

G. A. Lagoda, L. M. Su, and A. L. Burnett are with the Department of Urology, Johns Hopkins Medical Institutions, Baltimore, MD 21287 USA.

B. Electrical Nerve Stimulation

Identification of the CN was confirmed by electrical stimulation with simultaneous intracavernosal pressure (ICP) measurements. To assess ICP, the shaft of the penis was denuded of skin and the left crural region was cannulated with a 23-G needle connected via polyethylene tubing to a pressure transducer. To electrically stimulate the CN, a bipolar electrode attached to a Grass Instruments S48 stimulator was placed on top of the nerve. Stimulation parameters were 4 V for 60 s at a frequency of 16 Hz with a square wave duration of 5 ms. An increase in ICP after electrical stimulation of the CN was detected by a data acquisition system, and the response parameters were analyzed with MATLAB software.

C. Optical Nerve Stimulation

Laser stimulation of the CN was conducted with a continuous-wave, wavelength-tunable, Thulium fiber laser (TLT-5, IPG Photonics, Oxford, MA). A function generator and optical shutter were used to modulate the continuous-wave laser and produce pulsed output. The laser pulse duration, laser spot diameter, and stimulation time were fixed at 2.5 ms, 1 mm, and 60 s, respectively. The laser pulse energy was increased from 0.725 mJ – 6.75 mJ (0.09 - 0.86 J/cm^2). The laser pulse repetition rate was varied between 5-20 Hz. The laser wavelength was tuned between 1850-1880 nm, producing a variable optical penetration depth in the nerve from 300-600 micrometers, chosen to approximate the diameter of the rat CN. The laser beam was focused with a 200-mm-focal-length calcium fluoride lens into a 400-µm-core low-OH silica optical fiber. A green aiming beam was coupled into the fiber to provide alignment with the nerve. The working distance of the fiber tip from the nerve was kept fixed at 7 mm, providing a 1-mm-diameter spot (1/e^2) on the tissue surface, as measured using a razor blade scan. Table 1 summarizes the laser parameters studied. Figure 1 shows a diagram of the experimental setup.

TABLE I
OPTICAL STIMULATION PARAMETERS

Wavelength (nm):	1850 - 1880
Pulse Energy (mJ):	0.725 - 6.75
Spot Diameter (mm):	1
Fluence (J/cm^2):	0.09 - 0.86
Pulse Duration (ms):	2.5
Pulse Repetition Rate (Hz):	5 - 20

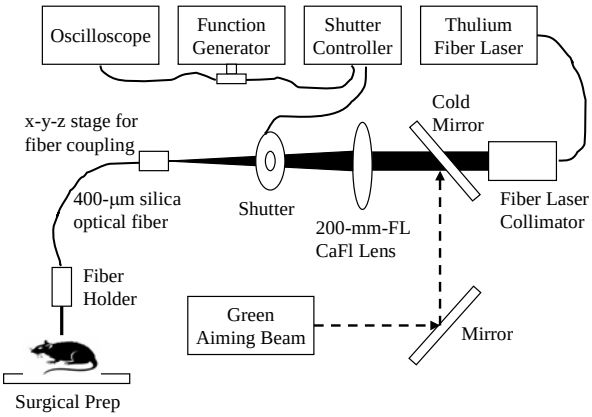

Fig. 1. Experimental setup for optical stimulation of the cavernous nerves.

D. Histological Preparation

At the completion of the study, the rats were euthanized by a lethal intracardiac injection of saturated potassium chloride while under anesthesia, as is consistent with the recommendations of the Panel of Euthanasia of the American Veterinary Medical Association. After euthanization, the CN was removed and fixed with a 10% formalin concentration. Cross-sections of the CN were processed for histological examination via hematoxylin and eosin staining.

III. RESULTS

The optimal laser stimulation parameters were observed at wavelengths of 1860-1870 nm, pulse energies greater than 2.7 mJ (0.35 J/cm^2), and a pulse rate of 10 Hz. Lower pulse energies and pulse rates failed to produce an ICP response during 60 s stimulation. After optimization of the laser stimulation parameters, ICP responses similar in magnitude to electrical stimulation were recorded, with no evidence of thermal damage to the nerves (Figures 2 and 3).

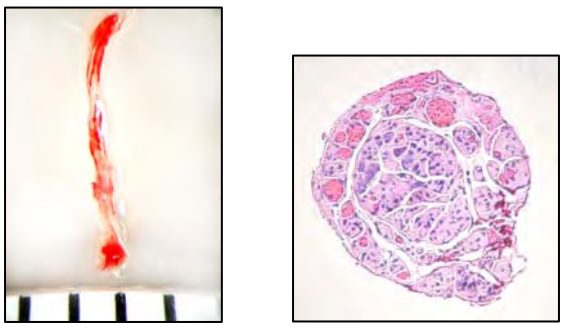

(a) (b)

Fig. 2. (a) Gross image of CN (bar = 1 mm) and (b) H&E-stained histologic cross-section of CN, after laser stimulation.

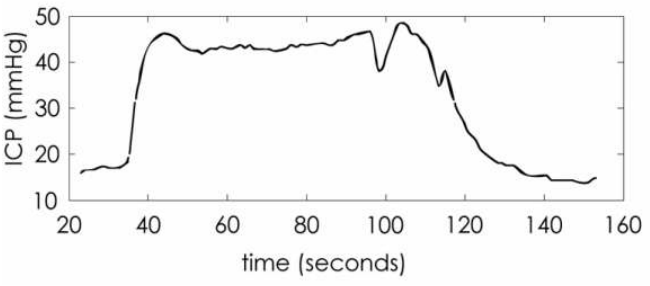

(a) Electrical stimulation (before)

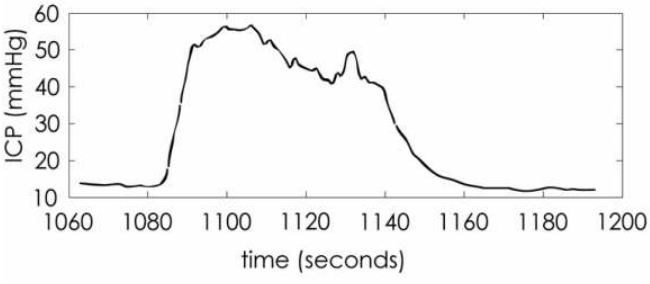

(b) Laser nerve stimulation

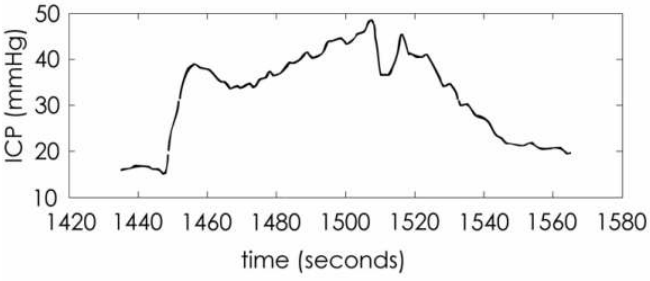

(c) Electrical stimulation (after)

Fig. 3. Intracavernosal pressure (ICP) response as a function of time for electrical and optical nerve stimulation over a period of 60 s. (a) Electrical stimulation at beginning of study; (b) Laser stimulation; (c) Electrical stimulation at end of study. A comparable ICP response is observed during electrical and laser stimulation, without evidence of loss in ICP signal or nerve function after repeated laser stimulation measurements.

However, as the pulse energy and/or pulse repetition rate were increased further, thermal damage to the nerve as evidenced by a significant loss in ICP response and gross and histological tissue analysis, was observed.

IV. DISCUSSION

There is a wide variability in reported sexual potency rates following prostate cancer surgery, due, in part, to the difficulty in preserving the CN during surgery. Any technology that can assist in identification and preservation of the CN during surgery may lead to direct patient benefit. Optical technologies are ideally suited for use in surgical guidance for several reasons. First, laser light may be delivered through small, flexible optical fibers and easily integrated into existing surgical instruments for potential use in laparoscopic and robotic nerve-sparing prostate cancer surgery. Second, lasers provide increased spatial resolution for stimulation of the nerves in comparison with electrical stimulation. Third, unlike electrical stimulation, lasers can stimulate the nerves in non-contact mode, thus avoiding potential mechanical damage to the nerve and interference with the surgeon's field-of-view during the procedure.

The purpose of this study was to use a rat prostate model to optimize the laser stimulation parameters as a potential diagnostic tool for identification of the CN during laparoscopic and robotic prostate cancer surgery. The rat CN is a relatively large, visible, and distinct structure as compared to its human counterpart, thus aiding identification. Furthermore, the rat prostate model allowed us to correlate laser nerve stimulation data with electrical nerve stimulation and histology.

However, a major limitation of this study is that the rat prostate model represents an idealized version of the human anatomy. In the rat, the CN is large and clearly visible as it courses along the prostate surface. In the human, on the contrary, although the CN courses near the prostate surface, there is intervening tissue (e.g. periprostatic fascia and cavernous blood vessels) between the nerves and the laser probe, making identification of the nerves more challenging.

V. CONCLUSION

The laser nerve stimulation parameters were optimized, resulting in an ICP response similar in magnitude and duration to conventional electrical stimulation. Noncontact optical stimulation of the cavernous nerves may represent an alternative to electrical nerve stimulation as a potential diagnostic tool during nerve-sparing laparoscopic and robotic prostate cancer surgery.

REFERENCES

[1] G. P. Murphy, C. Mettlin, H. Menck, D. P. Winchester, and A. M. Davidson, "National patterns of prostate cancer treatment by radical prostatectomy: results of a survey by the American College of Surgeons Committee on Cancer," *J. Urol.*, vol. 152, 1817-1819, 1994.

[2] J. A. Talcott, P. Rieker, K. J. Propert, J. A. Clark, K. I. Wishnow, K. R. Loughlin, J. P. Richie, and P. W. Kantoff, "Patient-reported impotence and incontinence after nerve-sparing radical prostatectomy," *J. Natl. Cancer Inst.*, vol. 89, pp. 1117-1123, 1997.

[3] V. E. Weldon, F. R. Tavel, and H. Neuwirth, Continence, potency and morbidity after radical perineal prostatectomy," *J. Urol.*, vol. 158:1470-1475, 1997.

[4] W. J. Catalona, G. F. Carvalhal, D. E. Mager, and D. S. Smith, "Potency, continence and complication rates in 1,870 consecutive radical retropubic prostatectomies," *J. Urol.*, vol. 162, pp. 433-438, 1999.

[5] P. C. Walsh, P. Marschke, D. Ricker, and A. L. Burnett, "Patient-reported urinary continence and sexual function after anatomic radical prostatectomy," *Urol.*, vol. 55, pp. 58-61, 2000.

[6] A. L. Burnett, G. Aus, E. D. Canby-Hagino, M. S. Cookson, A. V. D'Amico, R. R. Dmochowski, D. T. Eton, J. D. Forman, S. L. Goldenberg, J. Hernandez, C. S. Higano, S. Kraus, M. Liebert, J. W. Moul, C. Tangen, J. B. Thrasher, I. Thompson, "Erectile function outcome reporting after clinically localized prostate cancer treatment," *J. Urol.*, vol. 178(2), pp. 597-601, 2007.

[7] A. J. Costello, M. Brooks, and O. J. Cole, "Anatomical studies of the neurovascular bundle and cavernosal nerves," *BJU Int.*, vol. 94, pp. 1071-1076, 2004.

[8] M. Aron, J. H. Kaouk, N. J. Hegarty, J. R. Colombo, Jr., G. P. Haber, B. I. Chung, M. Zhou, I. S. Gill, "Preliminary experience with the Niris optical coherence tomography system during laparoscopic and robotic prostatectomy," *J. Endourol.*, vol. 21(8), pp. 814-818, 2007.

[9] N. M. Fried, S. Rais-Bahrami, G. A. Lagoda, Y. Chuang, A. L. Burnett, and L. M. Su, "Imaging the cavernous nerves in the rat prostate using optical coherence tomography," *Lasers Surg. Med.*, vol. 39, pp. 36-41, 2007.

[10] N. M. Fried, S. Rais-Bahrami, G. A. Lagoda, A. Y. Chuang, L. M. Su, and A. L. Burnett, "Identification and imaging of the nerves responsible for erectile function in rat prostate, in vivo, using optical nerve stimulation and optical coherence tomography," *IEEE J. Sel. Top. Quantum Electron.*, vol. 13(6), pp. 1641-1645, 2007.

[11] S. Rais-Bahrami, A. W. Levinson, N. M. Fried, G. A. Lagoda, A. Hristov, Y. Chuang, A. L. Burnett, and L. M. Su, "Optical coherence tomography of cavernous nerves: a step toward real-time intraoperative imaging during nerve-sparing radical prostatectomy," *Urol.* In press.

[12] D. Golijanin, R. W. Wood, R. R. Madeb, C. R. Silvers, J. L. Yao, J. Huang, E. M. Messing, J. E. Reeder, and J. V. Joseph, "Intraoperative visualization of cavernous nerves using near infrared fluorescence of indocyanine green in the rat," *J. Urol.*, vol. 175(4), p. 85, 2006.

[13] L. B. Boyette, M. A. Reardon, A. J. Mirelman, T. D. Kirkley, J. J. Lysiak, J. B. Tuttle, and W. D. Steers, "Fiberoptic imaging of cavernous nerves in vivo," *J. Urol.*, vol. 178(6), pp. 2694-2700, 2007.

[14] N. M. Fried, G. A. Lagoda, N. J. Scott, L. M. Su, and A. L. Burnett, "Non-contact stimulation of the cavernous nerves in the rat prostate using a tunable-wavelength thulium fiber laser," *J. Endourol.*, vol. 22(3), pp. 409-413, 2008.

[15] L. Klotz, "Neurostimulation during radical prostatectomy: improving nerve-sparing techniques," *Semin. Urol. Oncol.*, vol. 18, pp. 46-50, 2000.

[16] H. L. Kim, D. S. Stoffel, D. A. Mhoon, and C. B. Brendler, "A positive caver map response poorly predicts recovery of potency after radical prostatectomy," *Urol.*, vol. 56, pp. 561-564, 2000.

[17] L. Klotz, J. Heaton, M. Jewett, J. Chin, N. Fleshner, L. Goldenberg, and M. Gleave, "A randomized phase 3 study of intraoperative cavernous nerve stimulation with penile tumescence monitoring to improve nerve sparing during radical prostatectomy," *J. Urol.*, vol. 164, pp. 1573-1578, 2000.

[18] J. Holzbeierlein, M. Peterson, and J. A. Smith Jr, "Variability of results of cavernous nerve stimulation during radical prostatectomy," *J. Urol.*, vol. 165, pp. 108-110, 2001.

[19] P. C. Walsh, P. Marschke, W. J. Catalona, H. Lepor, S. Martin, R. P. Myers, and M. S. Steiner, "Efficacy of first-generation Cavermap to verify location and function of cavernous nerves during radical prostatectomy: a multi-institutional study by experienced surgeons," *Urol.*, vol. 57, pp. 491-494, 2001.

[20] H. L. Kim, D. A. Mhoon, and C. B. Brendler, "Does the CaverMap device help preserve potency?" *Curr. Urol. Rep.*, vol. 2, pp. 214-217, 2001.

[21] L. Klotz, "Cavernosal nerve mapping: current data and applications," *BJU Int.*, vol. 93, pp. 9-13, 2004.

[22] J. Wells, C. Kao, K. Mariappan, J. Albea, E. D. Jansen, P. Konrad, and A. Mahadevan-Jansen, "Optical stimulation of neural tissue in vivo," *Opt. Lett.*, vol. 30, pp. 504-506, 2005.

[23] J. Wells, C. Kao, E. D. Jansen, P. Konrad, and A. Mahadevan-Jansen, "Application of infrared light for in vivo neural stimulation," *J. Biomed. Opt.*, vol. 10:064003, pp. 1-11, 2005.

[24] A. D. Izzo, C. P. Richter, E. D. Jansen, and J. T. Walsh, "Laser stimulation of the auditory nerve," *Lasers Surg. Med.*, vol. 38, pp. 745-753, 2006.

[25] A. D. Izzo, J. T. Walsh, E. D. Jansen, M. Bendett, J. Webb, H. Ralph, and C. P. Richter, "Optical parameter variability in laser nerve stimulation: a study of pulse duration, repetition rate, and wavelength," *IEEE Trans. Biomed. Eng.*, vol. 54, pp. 1108-1114, 2007.

[26] J. D. Wells, S. Thomsen S, P. Whitaker, E. D. Jansen, C. C. Kao, P. E. Konrad, A. Mahadevan-Jansen, "Optical mediated nerve stimulation: identification of injury thresholds," *Lasers Surg. Med.* vol. 39, pp. 513-526, 2007.

Wavelet Denoising during Optical Coherence Tomography of the Prostate Nerves using the Complex Wavelet Transform

Shahab Chitchian, Michael Fiddy and Nathaniel M. Fried

***Abstract*— Preservation of the cavernous nerves during prostate cancer surgery is critical in preserving sexual function after surgery. Optical coherence tomography (OCT) of the prostate nerves has recently been studied for potential use in nerve-sparing prostate surgery. In this study, the discrete wavelet transform and complex dual-tree wavelet transform are implemented for wavelet shrinkage denoising in OCT images of the rat prostate. Applying the complex dual-tree wavelet transform provides improved results for speckle noise reduction in the OCT prostate image. Image quality metrics of the cavernous nerves and signal-to-noise ratio (SNR) were improved significantly using this complex wavelet denoising technique.**

I. Introduction

Improvements in real-time imaging and identification of the cavernous nerves during prostate cancer surgery would aid preservation of the nerves and improve postoperative sexual function.

Optical coherence tomography (OCT) is an emerging noninvasive optical imaging technique used to perform high-resolution cross-sectional *in vivo* and *in situ* imaging of microstructure in transparent and nontransparent biological tissues [1]. OCT imaging of the cavernous nerves in the rat and human prostate has recently been demonstrated [2], [3], [4], [5]. However, improvements in the quality of the OCT images may be necessary prior to clinical use.

Speckle occurs in the OCT image when the particles composed in the underlying tissue structures are smaller than the coherence length of the light source [6]. Speckle modeled as multiplicative noise can be transformed to additive noise by applying a logarithmic operation. Recently, wavelet techniques have been employed successfully in speckle noise reduction for OCT images [7].

Wavelet shrinkage denoising is denoising by nonlinear soft thresholding in the wavelet transform domain. The wavelet transform comes in several forms. The discrete wavelet transform (DWT) provides the most compact representation, however, it has several limitations. The dual-tree complex wavelet transform (CDWT) overcomes these limitations because it is nearly shift-invariant and is oriented in 2-D [8]. In this study, we compare the results of the discrete wavelet transform and dual-tree complex wavelet transform algorithms for wavelet shrinkage denoising in the OCT image of the rat prostate.

This research was supported in part by the Department of Energy, Grant#DE-FG02-06CH11460, an Idea Development Award from the Department of Defense Prostate Cancer Research Program, Grant #PC073709, and a Faculty Research Grant from the University of North Carolina at Charlotte.

S. Chitchian, M. Fiddy and N.M. Fried are with Department of Physics and Optical Science, University of North Carolina at Charlotte, NC 28223, USA (nmfried@uncc.edu).

II. Wavelet Shrinkage Denoising

Denoising attempts to remove noise and retain signal regardless of the frequency content of the signal. Wavelet shrinkage is denoising by shrinking (nonlinear soft thresholding) in the wavelet transform domain.

The observed image, X, is modeled as an uncorrupted image, S, and multiplicative speckle noise, N. On a logarithmic scale, speckle is converted to additive noise,

$$X = S + N \tag{1}$$

The wavelet shrinkage denoising algorithm requires the following four-step procedure [9], implemented by Matlab.

$$\begin{aligned} Y &= W(X) \\ \lambda &= d(Y) \\ Z &= D(Y, \lambda) \\ S &= W^{-1}(Z) \end{aligned} \tag{2}$$

III. Wavelet Transform

Wavelet transform is the representation of a function by scaled and translated copies of a finite-length or fast-decaying oscillating waveform, which can be used to analyze signals at multiple scales. Wavelet coefficients carry both time and frequency information, as the basis functions vary in position and scale.

A. 2-D Discrete Wavelet Transform

The discrete wavelet transform (DWT) converts a signal to its wavelet representation. In a one-level DWT, a signal c_0 is split into an approximation part c_1 and a detail part d_1. In a multilevel DWT, each subsequent c_i is split into an approximation c_{i+1} and detail d_{i+1}. For 2-D images, each c_i is split into an approximation c_{i+1} and three detail channels d^1_{i+1}, d^2_{i+1} and d^3_{i+1} for horizontally, vertically, and diagonally oriented details, respectively, Fig. 1. The inverse DWT (IDWT) reconstructs each c_i from c_{i+1} and d_{i+1}.

B. Complex 2-D Dual-Tree Wavelet Transform

The dual-tree complex wavelet transform (CDWT) calculates the complex transform of a signal using two separate DWT decompositions (tree a and tree b, Fig. 2). If the filters used in one are specifically designed different from those in the other it is possible for one DWT to produce the real coefficients and the other the imaginary. This redundancy of two provides extra information for analysis but at the expense of extra computational power.

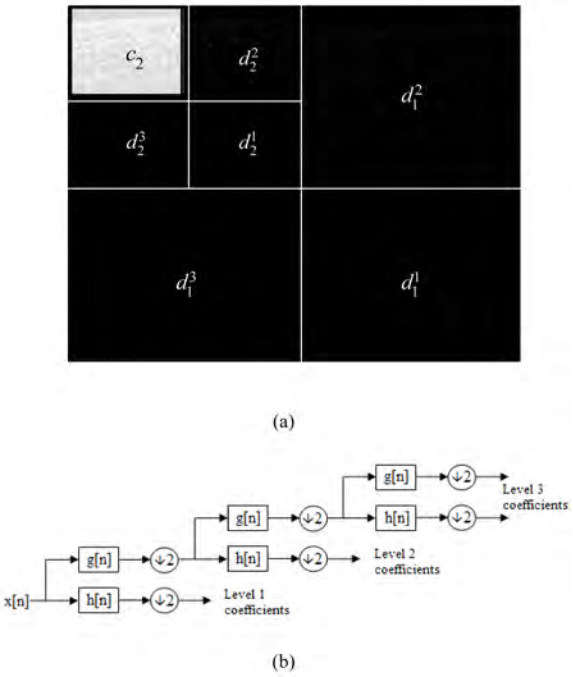

Fig. 1. (a) Ordering of the approximation and detail coefficients of two-level 2-D DWT. (b) A 3-level DWT wavelet filter bank.

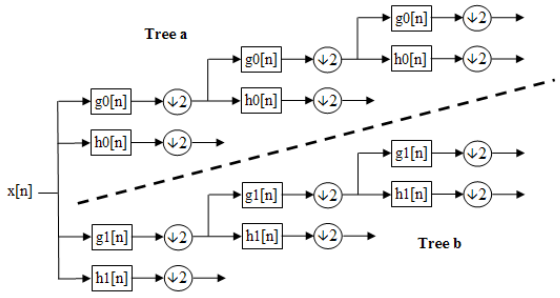

Fig. 2. Block diagram for a 3-level CDWT.

The wavelet transform, W, must be specified by its analysis and synthesis wavelet filter banks. In our case, wavelet coefficients are calculated from the Farras nearly symmetric wavelet [10]. The Wavelet Transform package by Selesnick *et al.* [11] was used for implementation of wavelet transform.

IV. Shrinkage Denoising

Operator $d(.)$ relates to the threshold procedure. In our case, it uses a single threshold globally for all relevant parts of the transform. VisuThresh as a practical, wavelet domain, global threshold procedure in which $\lambda = \sqrt{2 \log n}$ [12], is used for all levels of the transform.

$D(., \lambda)$ denotes the denoising operator with soft threshold λ. The following formula defines nonlinear soft thresholding for data Y [13],

$$D(Y, \lambda) \equiv sgn(Y) \times \max(0, |Y| - \lambda) \qquad (3)$$

D nulls all values of Y for which $|Y| \leq \lambda$ and shrinks toward the origin by an amount λ all values of Y for which $|Y| > \lambda$. It is the latter aspect that has led to D being called the shrinkage operator in addition to the soft thresholding operator. After estimating the signal components of the noisy coefficients in the wavelet domain, the inverse wavelet transform, W^{-1}, is taken to reconstruct the noise-free image.

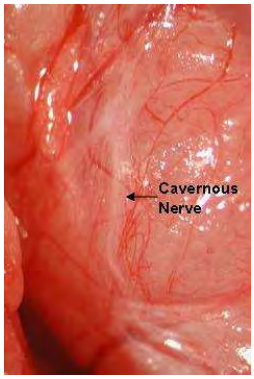

Fig. 3. Close-up view of the cavernous nerve on the surface of the rat prostate, shown in white.

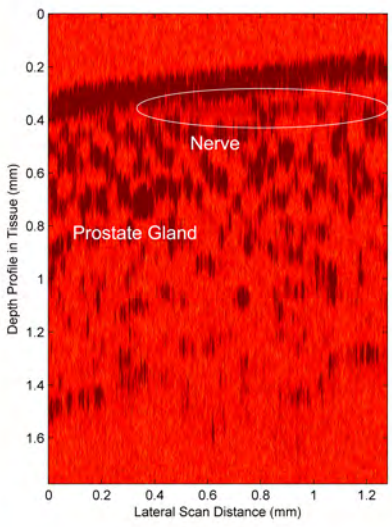

Fig. 4. OCT image of the rat cavernous nerve (Longitudinal section). The cavernous nerve lies superficial to the prostate gland.

V. Results and Discussion

Fig. 3 shows a close-up view of the cavernous nerve on the rat prostate. To demonstrate imaging, we performed two-dimensional cross-sectional OCT imaging of the rat prostate, Fig. 4. The resolution of the system is 20 μm (lateral) $\times$ 16 μm (longitudinal). The image size is 512$\times$512 pixels, covering an area of 1.3$\times$1.8 mm. The cavernous nerve can be differentiated from the surrounding periprostatic tissue and prostate gland.

The same OCT image from scanning the cavernous nerve coursing along the surface of the rat prostate after denoising is shown in Fig. 5 and Fig. 6. Wavelet shrinkage denoising

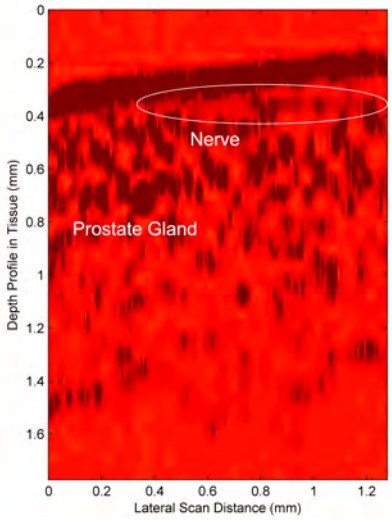

Fig. 5. OCT image of the rat cavernous nerve after wavelet shrinkage denoising using discrete wavelet transform (DWT).

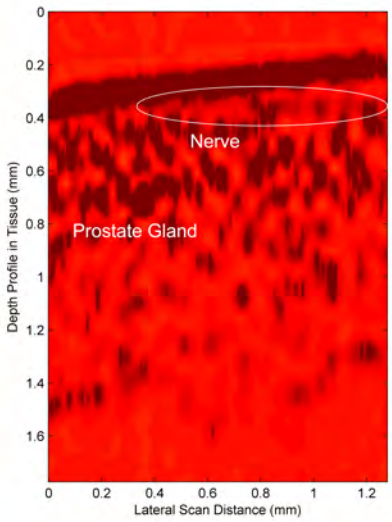

Fig. 6. OCT image of the rat cavernous nerve after wavelet shrinkage denoising using complex dual-tree wavelet transform (CDWT).

of the image can be compared using 2-D discrete wavelet transform, Fig. 5, and complex 2-D dual-tree wavelet transform, Fig. 6. The OCT signals in a longitudinal scan sample before and after filtering were also taken for comparison, Fig. 7.

The performances of these two wavelet transform procedures can be compared for the purpose of real-time image denoising and identification of the cavernous nerves in the prostate. The complex 2-D dual-tree wavelet transform performs visually better for denoising the image of the prostate nerves. Image quality metrics were also used to assess performance by measuring the average contrast-to-noise ratio (CNR) and the average equivalent number of looks (ENL) over the region of interest (ROI) which is the

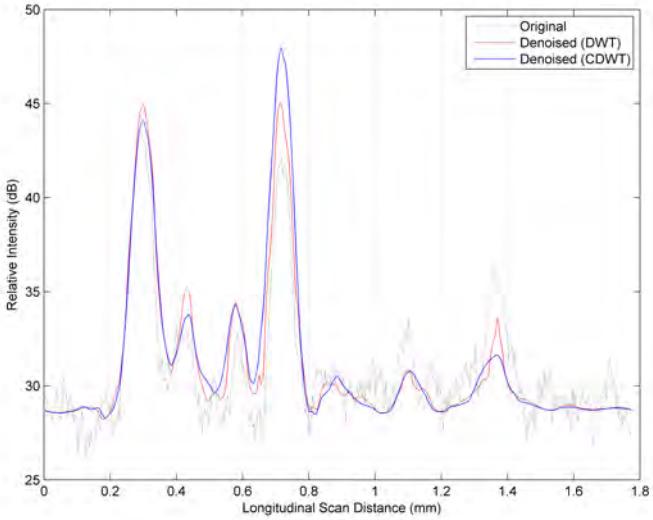

Fig. 7. Comparison of the OCT signals in a longitudinal scan sample before and after wavelet shrinkage denoising.

TABLE I
IMAGE QUALITY VALUES

Image	CNR (dB)	ENL	SNR (dB)
Original	0.4135	2439	37.61
Denoised(DWT)	5.23	5342	55.10
Denoised(CDWT)	5.71	6469	54.76

location of the cavernous nerve in each image. The CNR measures the contrast between an image feature and an area of background noise, while the ENL measures smoothness in areas that should have a homogeneous appearance but are corrupted by speckle. These image quality metrics are defined as the following [6], [7]:

$$CNR_n = 10 \times \log(\mu_n - \mu_b / \sqrt{\sigma_n^2 + \sigma_b^2}) \tag{4}$$

$$ENL_n = \mu_n^2 / \sigma_n^2 \tag{5}$$

where μ_n is the mean of the pixel values in the location of cavernous nerve, σ_n is the pixel standard deviation, and μ_b and σ_b are the pixel mean and standard deviation of a background region of the image, respectively. All measurements are made after logarithmic transformation.

In addition, the global SNR is calculated as [6]:

$$SNR = 10 \times \log(\max(X_{lin})^2 / \sigma_{lin}^2) \tag{6}$$

where X_{lin} is the two dimensional matrix of pixel values in the OCT image on a linear intensity scale and σ_{lin}^2 is the noise variance on a linear intensity scale. Table 1 shows image quality values for the original and wavelet denoised images.

The discrete wavelet transform lacks the shift-invariance property, and in multiple dimensions it performs poorly for distinguishing orientations, which is important in image processing. The complex 2-D dual-tree wavelet transform is

more selective with respect to orientation. It also provides approximate shift-invariance yet still allows perfect reconstruction of the signal. These properties make the complex dual-tree wavelet transform better in 2-D denoising than the normal discrete wavelet transform. CNR and ENL image quality metrics verify this, however, we can also visually recognize the advantage of shrinkage denoising using the complex dual-tree wavelet transform.

VI. Conclusion

The wavelet shrinkage denoising technique was used for speckle noise reduction in the OCT images of cavernous nerves in the rat prostate. Two different wavelet transform procedures were used: discrete wavelet transform and complex dual-tree wavelet transform, and their denoising results were compared for identification of the cavernous nerves. Image quality metrics improved significantly by those two algorithms. The complex dual-tree wavelet transform performs better visually and by numerical metrics for wavelet denoising in the OCT images of the prostate nerves.

VII. Acknowledgments

This research was supported in part by the Department of Energy, Grant#DE-FG02-06CH11460, an Idea Development Award from the Department of Defense Prostate Cancer Research Program, Grant #PC073709, and a Faculty Research Grant from the University of North Carolina at Charlotte.

References

[1] D. Huang, E. Swanson, C. Lin, J. Schuman, W. Stinson, W. Chang, M. Hee, T. Flotte, K. Gregory, C. Puliafito, and J. Fujimoto, "Optical coherence tomography," *Science*, vol. 254, pp. 1178–1181, 1991.

[2] M. Aron, J. Kaouk, N. Hegarty, J. Colombo, G. Haber, B. Chung, M. Zhou, and I. Gill, "Preliminary experience with the niris optical coherence tomography system during laparoscopic and robotic prostatectomy," *J. Endourol.*, vol. 21, no. 8, pp. 814–818, 2007.

[3] N. Fried, S. Rais-Bahrami, G. Lagoda, A. Chuang, A. Burnett, and L. Su, "Imaging the cavernous nerves in rat prostate using optical coherence tomography," *Lasers Surg. Med.*, vol. 39, no. 1, pp. 36–41, 2007.

[4] N. Fried, S. Rais-Bahrami, G. Lagoda, A. Chuang, L. Su, and A. Burnett, "Identification and imaging of the nerves responsible for erectile function in rat prostate, in vivo, using optical nerve stimulation and optical coherence tomography," *IEEE J. Sel. Top. Quant. Electron.*, vol. 13, no. 6, pp. 1641–1645, 2007.

[5] S. Rais-Bahrami, A. Levinson, N. Fried, G. Lagoda, A. Hristov, A. Chuang, A. Burnett, and L. Su, "Optical coherence tomography of cavernous nerves: A step toward real-time intraoperative imaging during nerve-sparing radical prostatectomy," *Urology*, In Press.

[6] J. Schmitt, S. Xiang, and K. Yung, "Speckle in optical coherence tomography," *J. Biomed. Opt.*, vol. 4, pp. 95–109, 1999.

[7] D. Adler, T. Ko, and J. Fujimoto, "Speckle reduction in optical coherence tomography images by use of a spatially adaptive wavelet filter," *Opt. Lett.*, vol. 29, pp. 2878–2880, 2004.

[8] N. Kingsbury, "Complex wavelets for shift invariant analysis and filtering of signals," *Applied and Computational Harmonic Analysis*, vol. 10, no. 3, pp. 234–253, 2002.

[9] C. Taswell, "The what, how, and why of wavelet shrinkage denoising," *Comput. Sci. Eng.*, vol. 2, pp. 12–19, 2000.

[10] A. F. Abdelnour and I. W. Selesnick, "Design of 2-band orthogonal near-symmetric cqf," in *Proc. IEEE Int. Conf. Acoust., Speech, Signal Processing (ICASSP)*, Salt Lake City, UT, USA, May 2001, pp. 3693–3696.

[11] S. Cai, K. Li, and I. Selesnick. (2003) Matlab implementation of wavelet transforms. [Online]. Available: http://taco.poly.edu/WaveletSoftware/

[12] D. Donoho and I. Johnstone, "Ideal spatial adaptation via wavelet shrinkage," *Biometrika*, vol. 81, pp. 425–455, 1994.

[13] D. Donoho, "De-noising by soft-thresholding," *IEEE Trans. Inform. Theory.*, vol. 41, pp. 613–627, 1995.

Design of a Compact Laparoscopic Probe for Optical Stimulation of the Cavernous Nerves

Serhat Tozburun[a] and Nathaniel M. Fried[ab]*

[a] Department of Physics and Optical Science, University of North Carolina at Charlotte, NC
[b] Department of Urology, Johns Hopkins Medical Institutions, Baltimore, MD

ABSTRACT

The cavernous nerves are responsible for erectile function and course along the prostate surface, varying in size and location among patients, making preservation of sexual function challenging after prostate cancer surgery. Electrical stimulation has proven inconsistent and unreliable in identifying these nerves and evaluating nerve function. Optical stimulation of the rat cavernous nerves has recently been reported as a alternative to electrical stimulation, with potential advantages including noncontact stimulation and improved spatial selectivity. This study describes the design of a compact laparoscopic probe for future clinical use in optical nerve stimulation. The 10-Fr (3.4-mm-OD) prototype laparoscopic probe includes an aspheric lens for collimation of the laser beam with a 0.8-mm-diameter spot, coupled with a 200-μm-core optical fiber. A 45° gold-coated rod mirror in the probe tip provides side-firing delivery of the laser radiation. The probe handle houses a miniature linear motorized stage for lateral scanning of the probe tip over a 25-mm line along the prostate surface. A 5.5-W Thulium fiber laser with tunable wavelength range of 1850-1880 nm was tested with the probe. The probe fits through a standard 5-mm-ID laparoscopic port and is capable of delivering pulse energies up to 8 mJ (1.6 J/cm^2) at a 2.5-ms pulse duration, well above the threshold (~ 0.35 J/cm^2) for optical stimulation of the cavernous nerves.

Key Words: optical stimulation, nerve, prostate, cavernous nerves, laparoscopic probe

1. INTRODUCTION

Preservation of the cavernous nerves during prostate cancer surgery is critical in preserving a man's ability to have spontaneous erections following surgery. Because of the close proximity of the nerves to the surface of the prostate, they are at risk of damage during dissection and removal of a cancerous prostate gland. As a result, there is a wide variability in reported potency rates following prostatectomy [1]. Improvements in identification of the cavernous nerves will likely aid in surgical preservation of the nerves during prostate surgery and lead to direct patient benefit.

Intra-operative electrical nerve mapping devices have been tested for preservation of the cavernous nerves during prostate surgery. However, these technologies have proven inconsistent and unreliable in identifying the nerves and evaluating nerve function [2]. Recently, optical nerve stimulation has been demonstrated using pulsed infrared lasers [3]. Laser nerve stimulation offers several general advantages over electrical stimulation, including non-contact method of stimulation, improved spatial selectivity, and elimination of stimulation artifacts.

Our laboratory previously reported successful optical stimulation of the cavernous nerves in a rat model [4,5]. We are developing this technique as a potential intra-operative diagnostic method for identifying and preserving the cavernous nerves during laparoscopic and robotic prostatectomy. There is a narrow range of parameters for nerve stimulation: a fluence less than ~ 0.35 J/cm^2 does not produce a reliable response, while a fluence above ~ 0.8-1 J/cm^2 results in nerve damage upon repetitive stimulation [5,6]. Since the fluence at the fiber output end may decrease rapidly due to beam divergence, it is critical that the probe produce a collimated beam over a short working distance (e.g. millimeters), so a constant fluence corresponding to safe and reproducible stimulation can be achieved.

The purpose of this study is to describe the design and assembly of a prototype laparoscopic probe for future clinical testing during nerve-sparing laparoscopic prostatectomy.

*nmfried@uncc.edu; phone: 1 704 687 8149; fax: 1 704 687 8197

Photonic Therapeutics and Diagnostics V, edited by Nikiforos Kollias, Bernard Choi, Haishan Zeng, Reza S. Malek, Brian Jet-Fei Wong, Justus F. R. Ilgner, Kenton W. Gregory, Guillermo J. Tearney, Laura Marcu, Henry Hirschberg, Steen J. Madsen, Proc. of SPIE Vol. 7161, 716113 · © 2009 SPIE · CCC code: 1605-7422/09/$18 · doi: 10.1117/12.807484

2. MATERIALS AND METHODS

The laparoscopic probe consists of several components (Figures 1 and 2). A standard probe from an existing disposable laparoscopic instrument was used to house a miniature linear motorized stage (MM-3M-F-1, National Aperture, inc., Salem, NH) capable of scanning for side-firing delivery a distance of 25 mm. The motorized stage was connected to a PC via USB connections and operated with Labview software. A 30-cm-long, stainless steel rod (2.7-mm-ID, 3.4-mm-OD, HTX-10R-24-05, Small Parts, inc., Miami Lakes, FL), capable of being inserted through a standard 5-mm-ID laparoscopic port was attached to the stage. This rod housed all of the optics inside a quartz capillary tube (2.0-mm-ID, 2.4-mm-OD, CV2024, Vitrocom, Mountain Lakes, NJ). The optics consisted of an aspheric lens (2-mm-OD, 350430-C, Thorlabs, Newton, NJ) and a 45° rod mirror (2-mm-OD, NT54-091, Edmund Optics, Barrington, NJ) with custom gold coating (International Micro Photonix, inc., Tewksbury, MA). A 200-μm-core low-OH silica optical fiber (BFL22-200, Thorlabs) with 0.22 NA was inserted into a glass ferrule (Vitrocom) for centering with the optics, and then glued into place inside the glass capillary tubing.

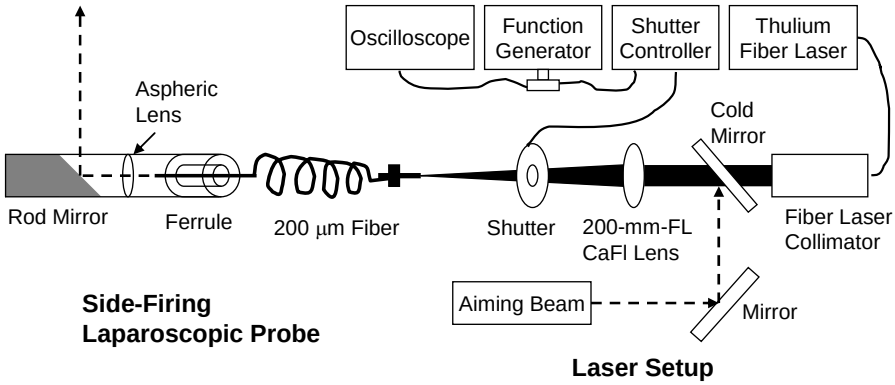

Figure 1. Diagram of experimental setup with fiber optic assembly for laser probe (left) and laser equipment (right).

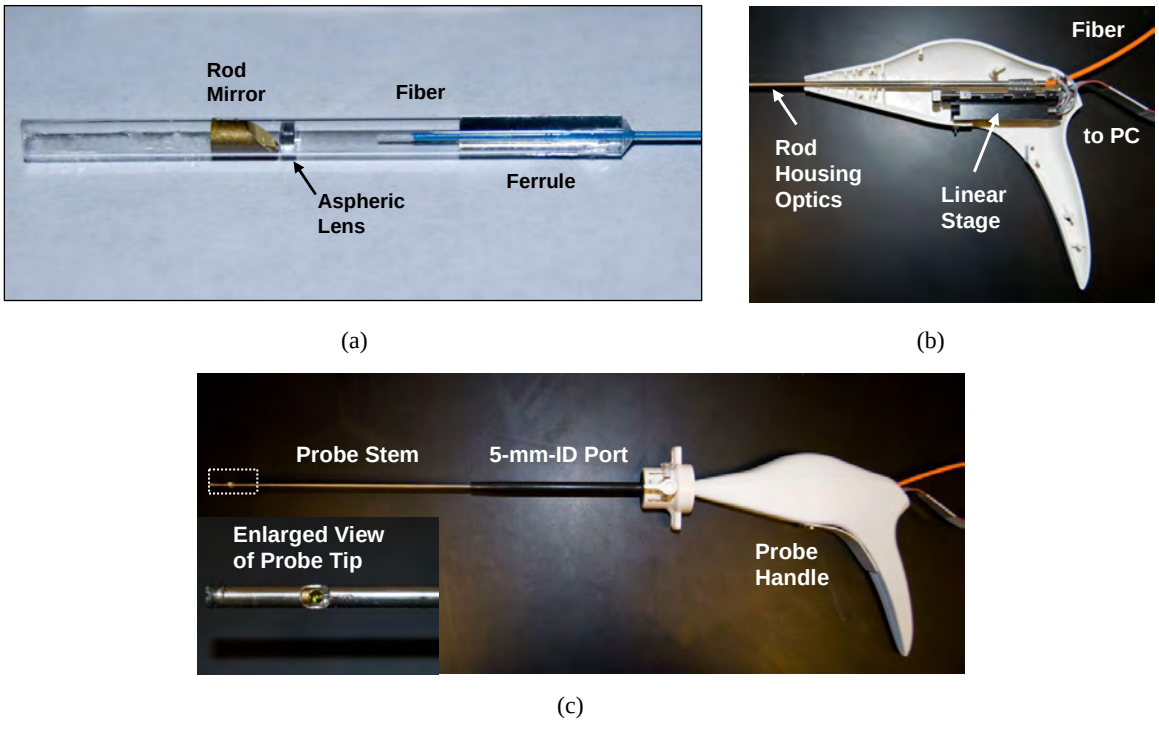

Figure 2. Probe design: (a) Optical component assembly; (b) Linear stage inside probe handle; (c) Assembled probe.

A 5.5-Watt Thulium fiber laser (TLT-5, IPG Photonics, Inc, Oxford, MA) with tunable wavelength range of 1850-1880 nm was tested with the probe. This relatively inexpensive, compact, portable laser source was chosen because its wavelength range provides an optical penetration depth in tissue that approximates the diameter of the cavernous nerve for uniform stimulation, and its excellent spatial beam profile allows efficient coupling of the laser energy into an optical fiber. The laser is capable of delivering pulse energies and fluences sufficient for optical nerve stimulation when externally modulated for operation in pulsed mode with a pulse length of approximately 2.5 ms.

3. RESULTS

Figure 3 shows preliminary studies designed to produce a collimated laser beam at the output end of the probe. The use of a smaller optical fiber diameter resulted in a more collimated laser beam (Figure 3a), as expected, but at the expense of greater transmission losses during coupling of the laser beam into the input end of the fiber. A 200-μm-core fiber provided a good compromise between an acceptable transmission rate of 64% (Table 1) and a collimated beam with a diameter of 0.8 mm over a distance of approximately 15-20 mm (Figure 3b), sufficient for use in laparoscopic surgery performed under magnification with a camera inserted through a separate port.

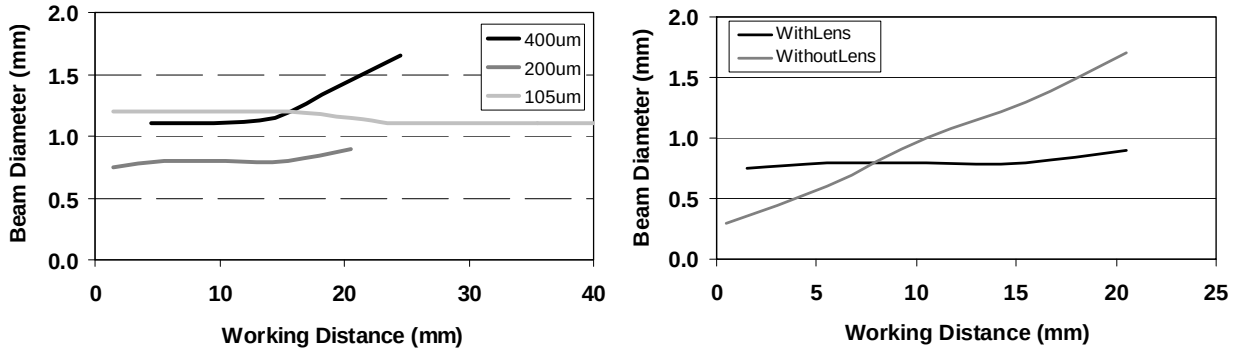

(a) (b)

Figure 3. (a) Divergence of laser beam as a function of fiber optic core diameter; (b) Comparison of beam divergence for 200 μm fiber without and without a collimating lens.

Figure 4ab shows the spatial beam profile in both 2D and 3D, acquired with an infrared beam analyzer (Pyrocam III, Spiricon, Logan UT). Figure 4c provides the $1/e^2$ Gaussian beam diameter measured with a razor blade scan.

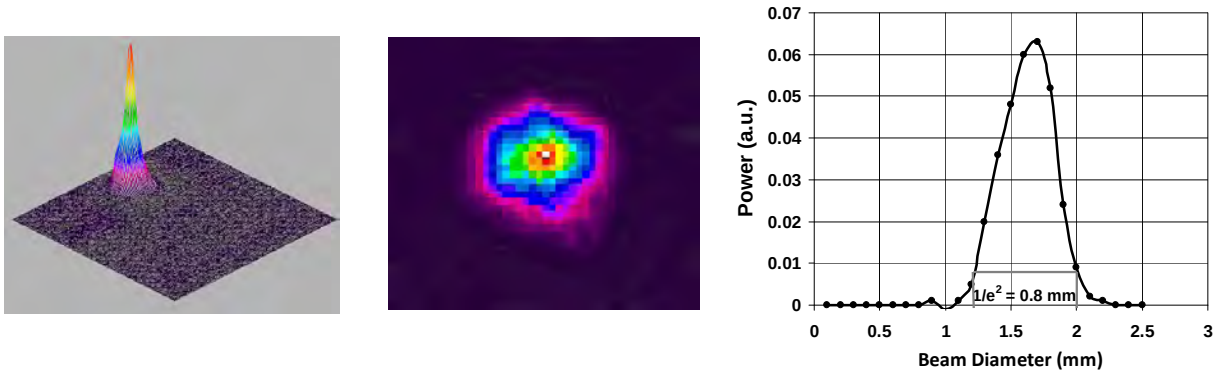

(a) (b) (c)

Figure 4. Spatial beam profile of the laser beam at the output end of the laparoscopic probe: (a) 3D profile; (b) Cross-section; (c) Razor blade scan of the $1/e^2$ beam diameter.

Table 1 provides a summary of the optical losses through the laser setup and laparoscopic probe optical components. The transmission rate out of the probe measured approximately 64%.

Table 1. Optical transmission losses measured as a function of optical components in probe and laser system.

Optical Component	Losses (%)
	100%
Laser system	
Cold Mirror:	- 11.9%
Focusing Lens:	- 5.8%
Optical Fiber:	- 7.9%
Probe	
Aspheric Lens:	- 4.5%
Rod Mirror + Tubing:	- 6.0%
Transmission:	**63.9%**

4. DISCUSSION

Optical stimulation of the cavernous nerves in a rat model has recently been demonstrated. This study describes the design and assembly of a laparoscopic probe for future testing during laser nerve stimulation in the clinic. Application of laser nerve stimulation in a clinical setting will require reproducible results. To provide optimal nerve stimulation without permanent damage to the nerves and loss of nerve function, the handheld probe needs to deliver a constant fluence at the tissue surface. Since optical fiber delivery is a requirement for such a device, and nerve stimulation is performed in a noncontact mode to preserve the surgical field-of-view, and the laser fluence at the output tip of the optical fiber normally decreases rapidly with beam expansion, optics are necessary to provide a collimated beam and fixed laser fluence over a short working distance. The laparoscopic laser probe described here provides a collimated laser beam over a short working distance of 15-20 mm.

5. CONCLUSIONS

A prototype compact laparoscopic probe was designed for future clinical testing of optical stimulation of the cavernous nerves during laparoscopic prostatectomy. The probe fits through a standard laparoscopic port, is capable of scanning a collimated 1-mm-diameter laser spot across the tissue surface, and delivering fluences sufficient for stimulation of the cavernous nerves.

6. ACKNOWLEDGMENTS

This research was supported by an Idea Development Award from the Department of Defense Prostate Cancer Research Program, Grant #PC073709.

REFERENCES

[1] Burnett, A. L., Aus, G., Canby-Hagino, E. D., Cookson, M. S., D'Amico, A. V., Dmochowski, R. R., Eton, D. T., Forman, J. D., Goldenberg, S. L., Hernandez, J., Higano, C. S., Kraus, S., Liebert, M., Moul, J. W., Tangen, C., Thrasher, J. B., and Thompson, I., "Erectile function outcome reporting after clinically localized prostate cancer treatment," J. Urol. 178(2), 597-601 (2007).

[2] Walsh, P. C., Marschke, P., Catalona, W. J., Lepor, H., Martin, S., Myers, R. P., and Steiner, M. S., "Efficacy of first-generation Cavermap to verify location and function of cavernous nerves during radical prostatectomy: a multi-institutional study by experienced surgeons," Urol., 57, 491-494 (2001).

[3] Wells, J., Kao, C., Jansen, E. D., Konrad, P., and Mahadevan-Jansen, A., "Application of infrared light for in vivo neural stimulation," J. Biomed. Opt. 10:064003, 1-11 (2005).

[4] Fried, N. M., Rais-Bahrami, S., Lagoda, G. A., Chuang, A. Y., Su, L. M., and Burnett, A. L., "Identification and imaging of the nerves responsible for erectile function in rat prostate, in vivo, using optical nerve stimulation and optical coherence tomography," IEEE J Sel Top Quantum Electron. 13(6), 1641-1645 (2007).

[5] Fried, N. M., Lagoda, G. A., Scott, N. J., Su, L. M., and Burnett, A. L., "Non-contact stimulation of the cavernous nerves in the rat prostate using a tunable-wavelength thulium fiber laser," J. Endourol. 22(3), 409-413 (2008).

[6] Wells, J. D., Thomsen, S., Whitaker, P., Jansen, E. D., Kao, C. C., Konrad, P. E., and Mahadevan-Jansen, A., "Optical mediated nerve stimulation: identification of injury thresholds," Lasers Surg. Med. 39, 513-526 (2007).

Speckle Reduction during All-Fiber Common-Path Optical Coherence Tomography of the Cavernous Nerves

Shahab Chitchian[a], Michael Fiddy[a], Nathaniel M. Fried[a,b]

[a] Department of Physics and Optical Science, University of North Carolina at Charlotte, NC
[b] Department of Urology, Johns Hopkins Medical Institutions, Baltimore, MD

ABSTRACT

Improvements in identification, imaging, and visualization of the cavernous nerves during prostate cancer surgery, which are responsible for erectile function, may improve nerve preservation and postoperative sexual potency. In this study, we use a rat prostate, *ex vivo*, to evaluate the feasibility of optical coherence tomography (OCT) as a diagnostic tool for real-time imaging and identification of the cavernous nerves. A novel OCT system based on an all single-mode fiber common-path interferometer-based scanning system is used for this purpose. A wavelet shrinkage denoising technique using Stein's unbiased risk estimator (SURE) algorithm to calculate a data-adaptive threshold is implemented for speckle noise reduction in the OCT image. The signal-to-noise ratio (SNR) was improved by 9 dB and the image quality metrics of the cavernous nerves also improved significantly.

Keywords: optical coherence tomography, cavernous nerves, wavelet shrinkage denoising

1. INTRODUCTION

Preservation of the cavernous nerves during radical prostatectomy for prostate cancer is critical in preserving a man's ability to have spontaneous erections following surgery. Because of the close proximity of the nerves to the prostate surface, they are at risk of injury during dissection and removal of a cancerous prostate gland. Their microscopic nature also makes it difficult to predict the true course and location of these nerves from one patient to another. These observations may explain in part the wide variability in reported potency rates following prostate cancer surgery.[1] Recent anatomical studies also suggest that the cavernous nerves may have more extensive branching along the prostate surface than originally thought, and that our current understanding of the location, extent, and course of these nerves may be limited.[2] Therefore, improvements in real-time imaging and identification of the cavernous nerves during surgery would aid preservation of the nerves and improve postoperative sexual potency, thus resulting in direct patient benefit.

Optical coherence tomography (OCT) is an emerging noninvasive optical imaging technique that can be used to perform high-resolution cross-sectional *in vivo* and *in situ* imaging of microstructure in transparent and nontransparent biological tissues.[3] OCT utilizes a low coherence (white light) interferometer to obtain cross-sectional images synthesized from a series of laterally adjacent depth-scans. OCT imaging of the cavernous nerves in the rat and human prostate has recently been demonstrated.[4–7] However, improvements in the quality of the OCT images may be necessary prior to clinical use.

Speckle occurs in the OCT image when the particles composed in the underlying structures are smaller than the coherence length of the light source.[8] Speckle modeled as multiplicative noise can be transformed to additive noise by applying a logarithmic operation. Many methods have been proposed to reduce speckle noise. However, those which use frequency and spatial compounding do not take advantage of the information contained in the speckle patterns and can be difficult to implement in real time.[9] Recently, wavelet techniques have been employed successfully in speckle noise reduction for OCT images.[10] Choosing a proper threshold algorithm for wavelet denoising is the main part of using wavelet techniques in speckle noise reduction. Stein's unbiased risk estimator (SURE) algorithm to calculate a data-adaptive threshold is the best practical threshold procedure for cases involving visual judgement of medical images.[11]

Further author information: (Send correspondence to Shahab Chitchian)
E-mail: schitchi@uncc.edu, Telephone: 1 704 687 8152, Fax: 1 704 687 8197

Optical Coherence Tomography and Coherence Domain Optical Methods in Biomedicine XIII,
edited by James G. Fujimoto, Joseph A. Izatt, Valery V. Tuchin, Proc. of SPIE Vol. 7168, 71682N
 · doi: 10.1117/12.807444

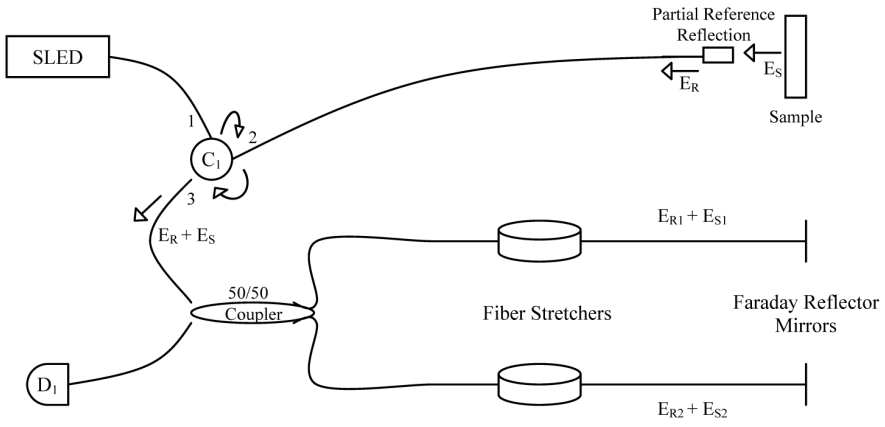

Figure 1. Common-path interferometer-based OCT system with the above configuration was used in tandem with a translational stage to obtain two-dimensional cross-sectional OCT images. SLED, C_1 and D_1 are the broadband light source, circulator and detector, respectively.

In this study, a novel, low-maintenance, low-cost, lightweight OCT system using an all single-mode fiber (SMF) common-path interferometer-based scanning system (Optiphase, Van Nuys, CA) is used for imaging and identification of the cavernous nerves in the rat prostate. The all SMF based interferometer provides a resolution comparable to bulk optics systems,[12] and may serve as a new low-cost OCT system for commercial applications.[13,14] A wavelet shrinkage denoising technique using SURE algorithm is applied for speckle noise reduction in the OCT image. It is shown that the image quality of the cavernous nerves improves both visually and by numerical metrics.

2. INTERFEROMETER DESIGN

The design of the common-path interferometer-based OCT system is shown in Figure 1. No separate arm for reference is required in the common-path-based OCT system, and this unique configuration provides the advantage of using any arbitrary length of detachable probe arm. The option to have detachable low-cost probes may simplify the instrumentation of endoscopic OCT (EOCT), and may also be very useful in cases where probes might need to be disposable to meet health safety standards.

3. EXPERIMENTAL OCT SETUP

In our experimental setup, the probe is mounted on a high-speed translational stage (850G-HS, Newport, Irvine, CA), interfaced with a motor controller (ESP 300, Newport, Irvine, CA) with the sample scanned in the transverse plane. The reflection from the air-glass interface of the fiber tip provides the reference signal and the piezoelectric fiber stretchers implement the longitudinal scanning function. The scan range of the system is 7 mm (in air) at a scanning frequency of 30 Hz. The Doppler frequency of the interferometer is approximately 695 kHz. Faraday mirrors are used instead of simple reflectors in the scanning interferometer to ensure high interferometric visibility, as well as to reverse the effects of polarization or birefringence modulation caused by sweeping the fiber stretchers.[15] This allows the entire design to be comprised of low-cost single-mode fiber. A superluminescent light-emitting diode (DL-CS 3504, DenseLight Semiconductors, Singapore) with a center wavelength of 1310 nm and 35 nm optical bandwidth was used as the light source. Our optical receiver (LDPF0065, Tyco Elec PINFET, with 80 kV/W sensitivity, 80 kΩ transimpedance at 1300 nm) has a saturation limit of approximately 25 W and a responsivity of approximately 0.8 A/W. OCT imaging was performed with an output power of 5 mW. The

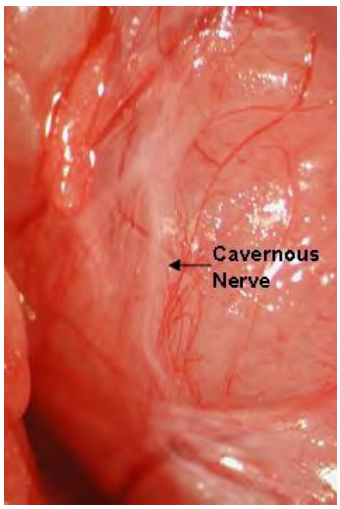

Figure 2. Close-up view of the cavernous nerve on the surface of the rat prostate, shown in white.

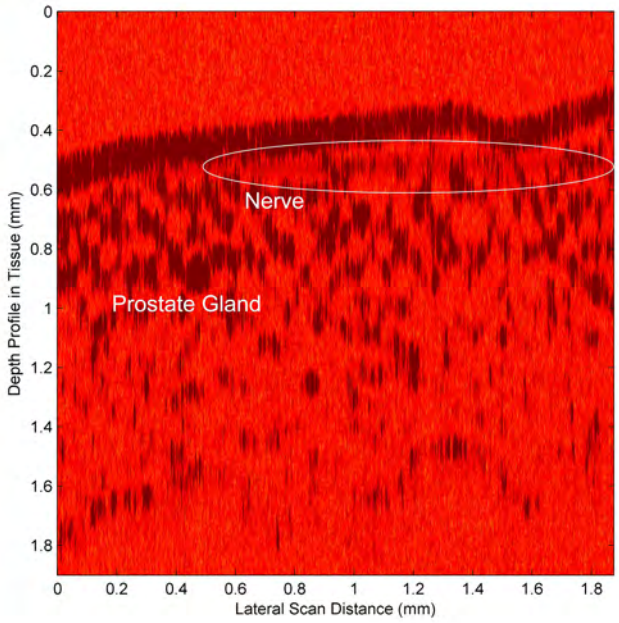

Figure 3. OCT image of the rat cavernous nerve (Longitudinal section). The cavernous nerve lies superficial to the prostate gland.

average SNR of our system is measured to be approximately 35 dB when a rat prostate sample is illuminated by 5 mW incident power.

Figure 2 shows a close-up view of the cavernous nerve on the rat prostate. Two-dimensional cross-sectional OCT imaging of the rat prostate was performed, Figure 3. The resolution of the system is 20 μm (lateral) $\times$ 16 μm (longitudinal). The image size is 750$\times$550 pixels, covering an area of 1.9$\times$1.9 mm.

4. WAVELET SHRINKAGE DENOISING

Although preliminary OCT imaging of the rat cavernous nerve was demonstrated based on this novel interferometer design, there is further need for improving the dynamic range of the system. In this section, wavelet

Table 1. Image Quality Values

Image	CNR (dB)	ENL	SNR (dB)
Original	-0.4519	2072	37.37
Denoised	2.225	3200	46.43

shrinkage denoising is employed to reduce the speckle noise in the OCT image. Denoising attempts to remove noise and retain signal regardless of the frequency content of the signal. Wavelet shrinkage is denoising by shrinking, nonlinear soft thresholding, in the wavelet transform domain. The observed image, X, is modeled as an uncorrupted image, S, and multiplicative speckle noise, N. On a logarithmic scale, speckle is converted to additive noise, $X = S+N$. The wavelet shrinkage denoising algorithm requires the following four-step procedure,[11] implemented by Matlab.

$$\begin{aligned} Y &= W(X) \\ \lambda &= d(Y) \\ Z &= D(Y,\lambda) \\ S &= W^{-1}(Z) \end{aligned} \tag{1}$$

A wavelet transform, W, must be specified by its analysis and synthesis wavelet filter banks. In our case, filter coefficients are calculated from the 8-tap Daubechies orthonormal wavelet with the total number of two-level 2-D wavelet transform.

Operator $d(.)$ selects a data-adaptive threshold which depends not just on the number of samples but on the data in any generic domain. We use the Stein's unbiased risk estimator (SURE) algorithm to calculate λ. SURE uses a local threshold λ_l estimated adaptively for each level l[16] and is the best threshold procedure that can be judged by human observer.[11] $D(.,\lambda)$ denotes the denoising operator with soft threshold λ, $D(Y,\lambda) \equiv sgn(Y) \times \max(0, |Y| - \lambda)$,.[17] D nulls all values of Y for which $|Y| \leq \lambda$ and shrinks toward the origin by an amount λ all values of Y for which $|Y| > \lambda$. After estimating the signal components of the noisy coefficients in the wavelet domain, the inverse wavelet transform, W^{-1}, is taken to reconstruct the noise-free image.

5. RESULTS AND DISCUSSION

The same OCT image from scanning the cavernous nerve coursing along the surface of the rat prostate after denoising is shown in Figure 4. In comparison with Figure 3, speckle noise reduction is observed after wavelet shrinkage denoising. The OCT signals in a longitudinal scan sample before and after filtering were also taken for comparison, Figure 5.

Image quality metrics were used to assess performance by measuring the average contrast-to-noise ratio, $CNR_n = 10 \times \log(\mu_n - \mu_b/\sqrt{\sigma_n^2 + \sigma_b^2})$,[8] and the average equivalent number of looks, $ENL_n = \mu_n^2/\sigma_n^2$,[10] over the region of interest which is the location of the cavernous nerve in each image. μ_n is the mean of the pixel values in the location of the cavernous nerve, σ_n is the pixel standard deviation, and μ_b and σ_b are the pixel mean and standard deviation of a background region of the image, respectively. All measurements are made after logarithmic transformation. In addition, the global SNR is calculated as $SNR = 10 \times \log(\max(X_{lin})^2/\sigma_{lin}^2)$, where X_{lin} is the two dimensional matrix of pixel values in the OCT image and σ_{lin}^2 is the noise variance, both on linear intensity scales.[8] Table 1 shows image quality values for the original and wavelet denoised images.

The SNR was improved by 9 dB in the rat prostate image. This is an improvement over the adaptive wavelet filtering algorithm used by Fujimoto et al (2004).[10] Identification of the cavernous nerves is performed visually during prostate cancer surgery. Therefore, we chose the SURE threshold procedure which has the best result for visual judgement.[11] The image quality was improved in the entire image and specifically in the region of the cavernous nerves.

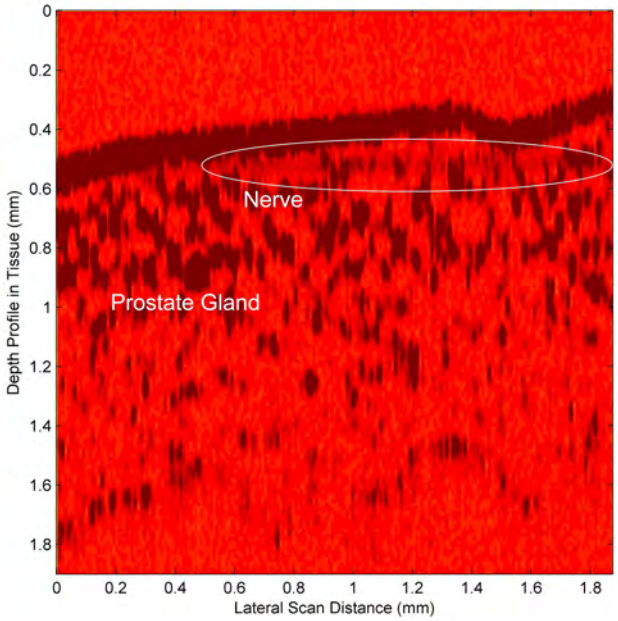

Figure 4. OCT image of the rat cavernous nerve after wavelet shrinkage denoising.

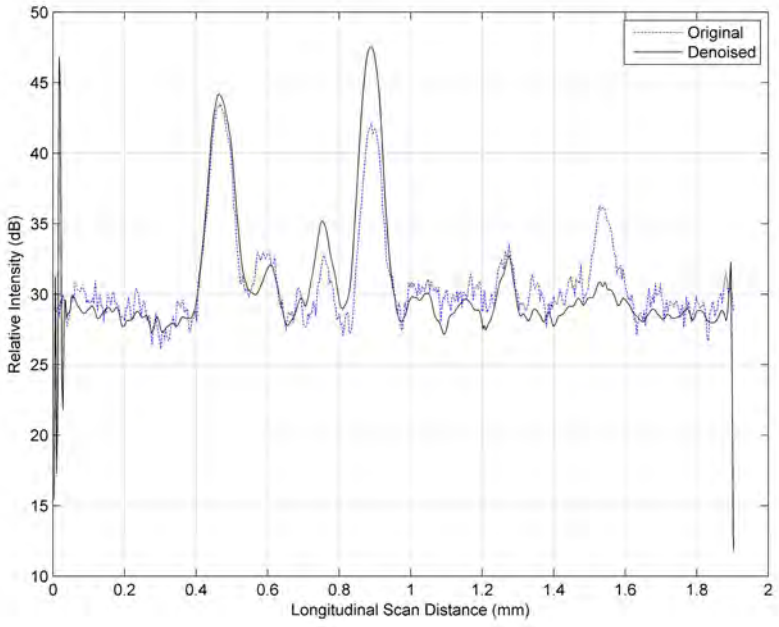

Figure 5. Comparison of the OCT signals in a longitudinal scan sample before and after wavelet shrinkage denoising.

6. CONCLUSION

A novel all-fiber common-path-based OCT system was used for imaging the cavernous nerves in the rat prostate, which is a relevant model for nerve-sparing prostate cancer surgery. The image quality was improved by applying wavelet shrinkage denoising using the Stein's unbiased risk estimator (SURE) algorithm to estimate a local threshold adaptively for any approximation and detail coefficients separately. A significant improvement in the image quality of the cavernous nerves and an SNR increase of 9 dB was obtained in the prostate image.

7. ACKNOWLEDGMENTS

This research was supported in part by the Department of Energy, Grant#DE-FG02-06CH11460, an Idea Development Award from the Department of Defense Prostate Cancer Research Program, Grant #PC073709, and a Faculty Research Grant from the University of North Carolina at Charlotte.

REFERENCES

[1] Burnett, A., Aus, G., Canby-Hagino, E., Cookson, M., D'Amico, A., Dmochowski, R., Eton, D., Forman, J., Goldenberg, S., Hernandez, J., Higano, C., Kraus, S., Liebert, M., Moul, j., Tangen, C., Thrasher, J., and Thompson, I., "Erectile function outcome reporting after clinically localized prostate cancer treatment," *J. Urol.* **178**(2), 597–601 (2007).

[2] Costello, A., Brooks, M., and Cole, O., "Anatomical studies of the neurovascular bundle and cavernosal nerves," *BJU Int.* **94**, 1071–1076 (2004).

[3] Huang, D., Swanson, E., Lin, C., Schuman, J., Stinson, W., Chang, W., Hee, M., Flotte, T., Gregory, K., Puliafito, C., and Fujimoto, J., "Optical coherence tomography," *Science* **254**, 1178–1181 (1991).

[4] Aron, M., Kaouk, J., Hegarty, N., Colombo, J., Haber, G., Chung, B., Zhou, M., and Gill, I., "Preliminary experience with the niris optical coherence tomography system during laparoscopic and robotic prostatectomy," *J. Endourol.* **21**(8), 814–818 (2007).

[5] Fried, N., Rais-Bahrami, S., Lagoda, G., Chuang, A., Burnett, A., and Su, L., "Imaging the cavernous nerves in rat prostate using optical coherence tomography," *Lasers Surg. Med.* **39**(1), 36–41 (2007).

[6] Fried, N., Rais-Bahrami, S., Lagoda, G., Chuang, A., Su, L., and Burnett, A., "Identification and imaging of the nerves responsible for erectile function in rat prostate, in vivo, using optical nerve stimulation and optical coherence tomography," *IEEE J. Sel. Top. Quant. Electron.* **13**(6), 1641–1645 (2007).

[7] Rais-Bahrami, S., Levinson, A., Fried, N., Lagoda, G., Hristov, A., Chuang, A., Burnett, A., and Su, L., "Optical coherence tomography of cavernous nerves: A step toward real-time intraoperative imaging during nerve-sparing radical prostatectomy," *J. Urol.* , online publication (2008).

[8] Schmitt, J., Xiang, S., and Yung, K., "Speckle in optical coherence tomography," *J. Biomed. Opt.* **4**, 95–109 (1999).

[9] Xiang, S., Zhou, L., and Schmitt, J., "Speckle noise reduction for optical coherence tomography," *SPIE Proc.* **3196**, 79–88 (1997).

[10] Adler, D., Ko, T., and Fujimoto, J., "Speckle reduction in optical coherence tomography images by use of a spatially adaptive wavelet filter," *Opt. Lett.* **29**, 2878–2880 (2004).

[11] Taswell, C., "The what, how, and why of wavelet shrinkage denoising," *Comput. Sci. Eng.* **2**, 12–19 (2000).

[12] Bush, J., Davis, P., and Marcus, M., "All-fiber optic coherence domain interferometric techniques," *SPIE Proc.* **4204**, 71–80 (2000).

[13] Feldchtein, F., Bush, J., Gelikonov, G., Gelikonov, V., and Piyevsky, S., "Cost-effective, all-fiber autocorrelator based 1300 nm oct system," *SPIE Proc.* **5690**, 349–354 (2005).

[14] Sharma, U., Fried, N., and Kang, J., "All-fiber common-path optical coherence tomography: sensitivity optimization and system analysis," *IEEE J. Sel. Top. Quant. Electron.* **11**, 799–805 (2005).

[15] Kersey, A., Marrone, M., and Davis, M., "Polarization insensitive fiber optic michelson interferometer," *Electron. Lett.* **27**(6), 518–519 (1991).

[16] Donoho, D. and Johnstone, I., "Adapting to unknown smoothness via wavelet shrinkage," *J. Amer. Stat. Assoc.* **90**, 1200–1224 (1995).

[17] Donoho, D., "De-noising by soft-thresholding," *IEEE Trans. Inform. Theory.* **41**, 613–627 (1995).

Denoising during Optical Coherence Tomography of the Prostate Nerves via Bivariate Shrinkage using Dual-Tree Complex Wavelet Transform

Shahab Chitchian[a], Michael Fiddy[a], Nathaniel M. Fried[a,b]

[a] Department of Physics and Optical Science, University of North Carolina at Charlotte, NC
[b] Department of Urology, Johns Hopkins Medical Institutions, Baltimore, MD

ABSTRACT

The performance of wavelet shrinkage algorithms for image-denoising can be improved significantly by considering the statistical dependencies among wavelet coefficients as demonstrated by several algorithms presented in the literature. In this paper, a locally adaptive denoising algorithm using a bivariate shrinkage function is applied to reduce speckle noise in time-domain (TD) optical coherence tomography (OCT) images of the prostate. The algorithm is illustrated using the dual-tree complex wavelet transform. The cavernous nerve and prostate gland can be separated from discontinuities due to noise, and image quality metrics improvements with signal-to-noise ratio (SNR) increase of 14 dB are attained with a sharpness reduction of only 3%.

1. INTRODUCTION

Optical coherence tomography (OCT) is a noninvasive optical imaging technique used to perform high-resolution cross-sectional *in vivo* and *in situ* imaging of microstructure in biological tissues.[1] OCT imaging of the cavernous nerves in the rat and human prostate has recently been demonstrated.[2–5] However, improvements in the quality of the images for identification of the cavernous nerves during prostate cancer surgery would aid preservation of the nerves and improve postoperative sexual function. Speckle occurs in the OCT image when the particles composed in the underlying tissue structures are smaller than the coherence length of the light source.[6] Recently, wavelet techniques have been employed successfully in speckle noise reduction for OCT images.[7] Wavelet shrinkage denoising is denoising by nonlinear soft thresholding in the wavelet transform domain. In this paper, a local adaptive estimation of necessary parameters for a bivariate shrinkage function is applied on the dual-tree complex wavelet transform for wavelet shrinkage denoising in the OCT images of the rat prostate. Comparisons before and after image-denoising are given to illustrate the effectiveness of this approach.

2. LOCAL ADAPTIVE ALGORITHM

In the wavelet domain the denoising problem can be formulated as $\mathbf{y} = \mathbf{w} + \mathbf{n}$, where $\mathbf{w} = (w_1, w_2)$, $\mathbf{y} = (y_1, y_2)$ and $\mathbf{n} = (n_1, n_2)$. w_2 is the wavelet coefficient at the same position as w_1, but at the next coarser scale. The MAP estimator of w_1 can be used as[8]

$$\hat{w}_1 = \frac{(\sqrt{y_1^2 + y_2^2} - \frac{\sqrt{3}\sigma_n^2}{\sigma})_+}{\sqrt{y_1^2 + y_2^2}} \cdot y_1 \tag{1}$$

which can be interpreted as a bivariate shrinkage function. A robust median estimator is applied to estimate the noise variance σ_n^2 from the finest scale wavelet coefficients[9]

$$\hat{\sigma}_n^2 = \frac{median(|y_i|)}{0.6745}, \quad y_i \in subband\ \ HH. \tag{2}$$

Further author information: (Send correspondence to Shahab Chitchian)
E-mail: schitchi@uncc.edu, Telephone: 1 704 687 8152, Fax: 1 704 687 8197

Photonic Therapeutics and Diagnostics V, edited by Nikiforos Kollias, Bernard Choi, Haishan Zeng, Reza S. Malek, Brian Jet-Fei Wong, Justus F. R. Ilgner, Kenton W. Gregory, Guillermo J. Tearney, Laura Marcu, Henry Hirschberg, Steen J. Madsen, Proc. of SPIE Vol. 7161, 716112 · © 2009 SPIE · CCC code: 1605-7422/09/$18 · doi: 10.1117/12.807438

Table 1. Mean Values of Image Quality Metrics

Image	CNR (dB)	ENL	β (%)	SNR (dB)
Original	8.31	1613.9	100	26.65
Denoised	11.47	2466.8	97	40.87

The marginal variance σ^2 for the kth coefficient will be estimated using neighboring coefficients within a square-shaped window $N(k)$ which is centered at the kth coefficient. From the model, $\sigma_y^2 = \sigma^2 + \sigma_n^2$ where σ_y^2 is the marginal variance of noisy data y_1 and y_2. Since y_1 and y_2 are modeled as zero mean, σ_y^2 can be found empirically by[10]

$$\hat{\sigma}_y^2 = \frac{1}{M}\sum y_i^2, \quad y_i \in N(k) \tag{3}$$

where M is the size of neighboring coefficients, $N(k)$. Then, σ can be estimated as

$$\hat{\sigma} = \sqrt{(\hat{\sigma}_y^2 - \hat{\sigma}_n^2)_+}. \tag{4}$$

The Wavelet Transform package by Selesnick *et al.*[11] was used for implementation of the following summarized algorithm.

1. Calculate the noise variance $\hat{\sigma}_n^2$ using (2).
2. For each wavelet coefficient:
   a) Calculate $\hat{\sigma}_y^2$ using (3).
   b) Calculate $\hat{\sigma}$ using (4).
   c) Estimate each coefficient using $\hat{\sigma}$ and $\hat{\sigma}_n^2$ in (1).

3. RESULTS

TD OCT images of the cavernous nerves coursing along the surface of the rat prostate at different orientations (longitudinal, oblique, and cross-sectional) were taken by an FDA-approved, clinical endoscopic OCT system (Imalux, Cleveland, OH). Figure 1 shows these images before and after denoising.

Image quality metrics were used to assess performance by measuring the average contrast-to-noise ratio, $CNR_n = 10 \times \log(\mu_n - \mu_b/\sqrt{\sigma_n^2 + \sigma_b^2})$,[6] and the average equivalent number of looks, $ENL_n = \mu_n^2/\sigma_n^2$,[7] over the region of interest which is the location of the cavernous nerve in each image. μ_n is the mean of the pixel values in the location of the cavernous nerve, σ_n is the pixel standard deviation, and μ_b and σ_b are the pixel mean and standard deviation of a background region of the image, respectively. All calculations are made after logarithmic transformation of the image. In addition, the global SNR is calculated as $SNR = 10 \times \log(\max(X_{lin})^2/\sigma_{lin}^2)$, where X_{lin} is the two dimensional matrix of pixel values in the OCT image and σ_{lin}^2 is the noise variance, both on linear intensity scales.[6] The image sharpness parameter, β, determines the degree of smoothing in the denoised image in the location of the cavernous nerve.[12] The mean values of CNR, ENL and SNR for 9 sample images show significant improvement with a slight reduction in the β, as shown in Table 1.

4. CONCLUSION

A bivariate shrinkage model was applied to the wavelet denoising for speckle noise reduction in TD OCT images of the prostate gland. The dual-tree complex wavelet transform was used to take advantage of this transform which is shift-invariant and directionally selective. An SNR increase of 14 dB with significant image quality improvements was obtained. This algorithm for wavelet denoising may be a useful technique for clinical OCT applications.

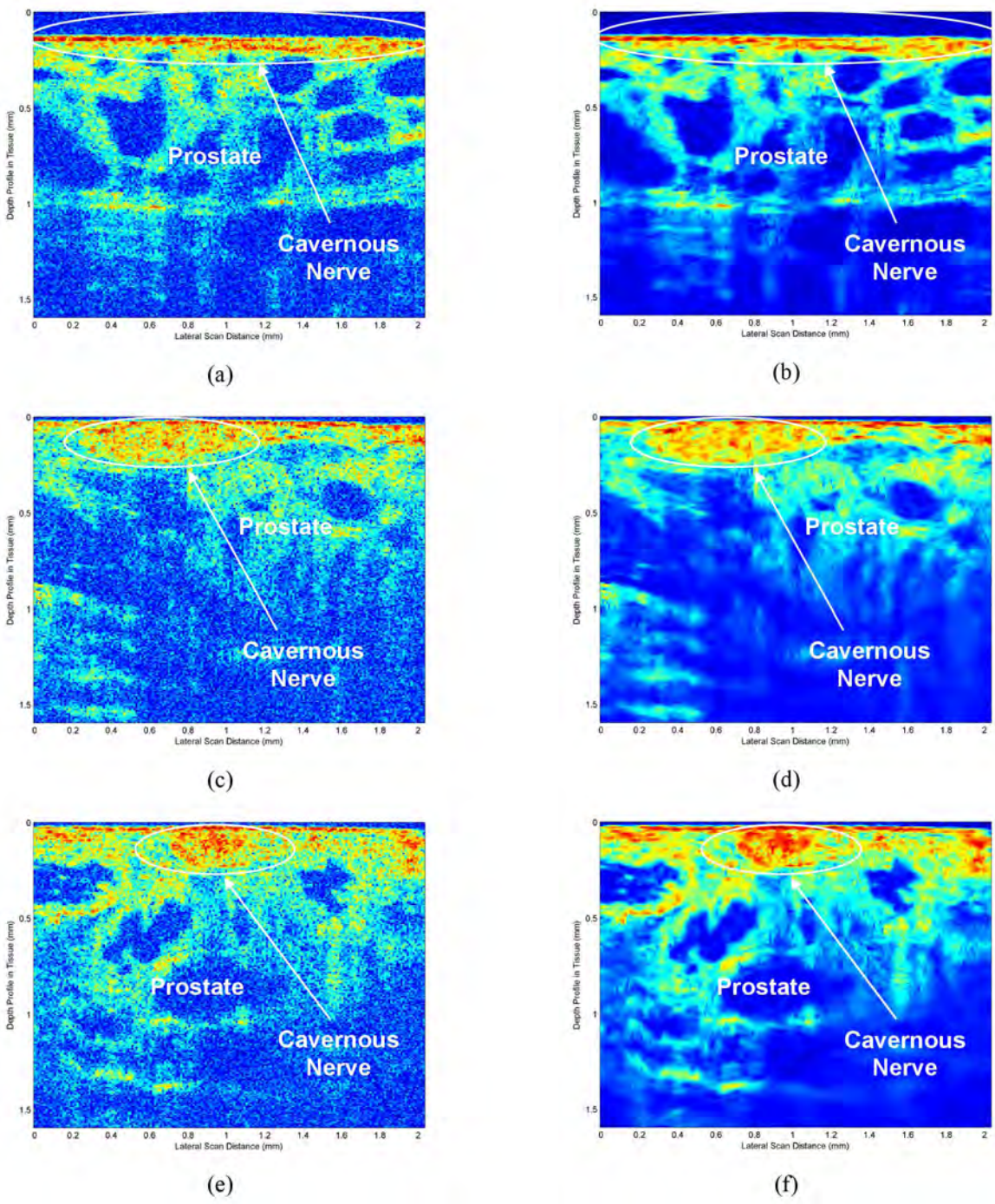

Figure 1. TD OCT images of the rat cavernous nerve: (a,b) Longitudinal section; (c,d) Oblique section; (e,f) Cross-section. (a,c,e) before; (b,d,f) after denoising. The cavernous nerve, corresponding to a relatively high signal intensity (shown in red), lies superficial to the prostate gland.

5. ACKNOWLEDGMENTS

This research was supported in part by the Department of Energy, Grant#DE-FG02-06CH11460, an Idea Development Award from the Department of Defense Prostate Cancer Research Program, Grant #PC073709, and a Faculty Research Grant from the University of North Carolina at Charlotte. The authors thank Nancy Tresser of Imalux Corporation (Cleveland, OH) for lending us the Niris OCT system for these studies.

REFERENCES

[1] Huang, D., Swanson, E., Lin, C., Schuman, J., Stinson, W., Chang, W., Hee, M., Flotte, T., Gregory, K., Puliafito, C., and Fujimoto, J., "Optical coherence tomography," *Science* **254**, 1178–1181 (1991).

[2] Aron, M., Kaouk, J., Hegarty, N., Colombo, J., Haber, G., Chung, B., Zhou, M., and Gill, I., "Preliminary experience with the niris optical coherence tomography system during laparoscopic and robotic prostatectomy," *J. Endourol.* **21**(8), 814–818 (2007).

[3] Fried, N., Rais-Bahrami, S., Lagoda, G., Chuang, A., Burnett, A., and Su, L., "Imaging the cavernous nerves in rat prostate using optical coherence tomography," *Lasers Surg. Med.* **39**(1), 36–41 (2007).

[4] Fried, N., Rais-Bahrami, S., Lagoda, G., Chuang, A., Su, L., and Burnett, A., "Identification and imaging of the nerves responsible for erectile function in rat prostate, in vivo, using optical nerve stimulation and optical coherence tomography," *IEEE J. Sel. Top. Quant. Electron.* **13**(6), 1641–1645 (2007).

[5] Rais-Bahrami, S., Levinson, A., Fried, N., Lagoda, G., Hristov, A., Chuang, A., Burnett, A., and Su, L., "Optical coherence tomography of cavernous nerves: A step toward real-time intraoperative imaging during nerve-sparing radical prostatectomy," *J. Urol.* (online, 15 February 2008).

[6] Xiang, S., Zhou, L., and Schmitt, J., "Speckle noise reduction for optical coherence tomography," *Proc. SPIE* **3196**, 79–88 (1997).

[7] Adler, D., Ko, T., and Fujimoto, J., "Speckle reduction in optical coherence tomography images by use of a spatially adaptive wavelet filter," *Opt. Lett.* **29**, 2878–2880 (2004).

[8] Sendur, L. and Selesnick, I., "Bivariate shrinkage functions for wavelet-based denoising exploiting interscale dependency," *IEEE Trans. Signal Processing* **50**(11), 2744–2756 (2002).

[9] Donoho, D. and Johnstone, I., "Ideal spatial adaptation via wavelet shrinkage," *Biometrika* **81**, 425–455 (1994).

[10] Sendur, L. and Selesnick, I., "Bivariate shrinkage with local variance estimation," *IEEE Signal Processing Letters* **9**(12), 438–441 (2002).

[11] Selesnick, I., Cai, S., Li, K., Sendur, L., and Abdelnour, A., "Matlab implementation of wavelet transforms," http://taco.poly.edu/WaveletSoftware/.

[12] Sattar, F., Floreby, L., Salomonsson, G., and Lovstrom, B., "Image enhancement based on a nonlinear multiscale method," *IEEE Trans. Image Processing* **6**, 888–895 (1997).

NONCONTACT OPTICAL STIMULATION OF THE CAVERNOUS NERVES IN THE RAT PROSTATE: OPTIMIZATION OF THE LASER PARAMETERS

Nathaniel M. Fried[1,2], Gwen A. Lagoda[2], Nicholas J. Scott[1], Li-Ming Su[2], and Arthur L. Burnett[2]

[1] Department of Physics and Optical Science, University of North Carolina at Charlotte, NC
[2] Department of Urology, Johns Hopkins Medical Institutions, Baltimore, MD

Introduction: Optical stimulation of nerves using near-infrared laser radiation has recently been demonstrated as an alternative to electrical stimulation. Advantages include non-contact stimulation, improved spatial selectivity, and elimination of electrical stimulation artifacts. This study explores laser stimulation of the rat cavernous nerves as a potential diagnostic tool for identification and preservation of the nerves during radical prostatectomy. The affect of laser wavelength, pulse energy, and pulse rate on nerve stimulation are studied to produce the maximum response in intracavernosal pressure (ICP).

Methods: The cavernous nerves were surgically exposed in a total of 10 rats. A Thulium fiber laser was used for nerve stimulation. The laser pulse duration, laser spot diameter, and stimulation time were fixed at 2.5 ms, 1 mm, and 60 s, respectively. The laser wavelength was tuned between 1850-1880 nm, producing a variable optical penetration depth in the nerve from 300-600 micrometers. The laser pulse energy was increased from 0.725 mJ – 6.75 mJ (0.09 - 0.86 J/cm^2). The laser pulse repetition rate was varied between 5-20 Hz. Electrical nerve stimulation was also performed for comparison (Figure 1).

Results: The optimal laser stimulation parameters were observed to be at wavelengths of 1860-1870 nm, pulse energies greater than 2.7 mJ (0.35 J/cm^2), and a pulse repetition rate of approximately 10 Hz. Lower pulse energies and repetition rates below the threshold for optical stimulation produced no observable ICP response during 60 s stimulation. As the pulse energy and repetition rate was increased further, thermal damage to the nerve and loss of ICP response was more frequently observed.

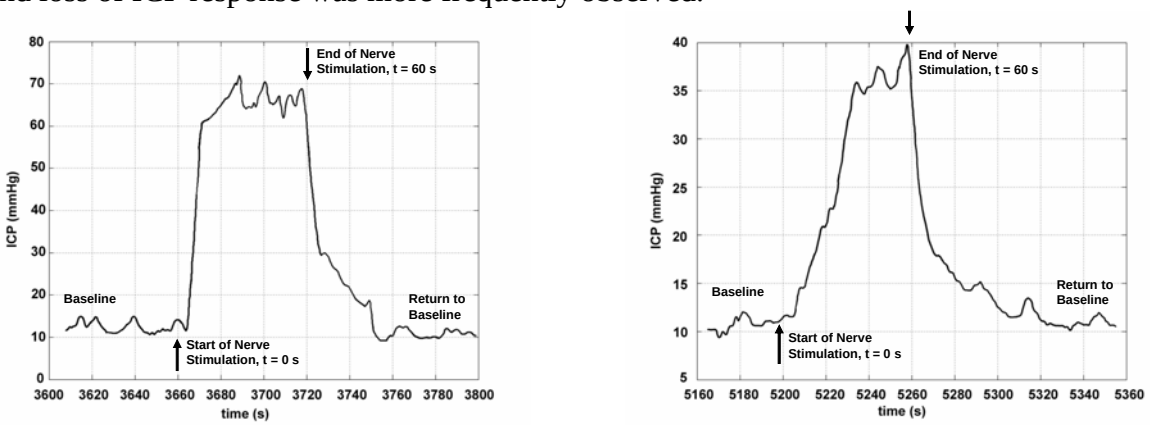

Figure 1. Representative intracavernosal pressure (ICP) response after (a) electrical and (b) optical nerve stimulation.

Conclusions: Noncontact optical stimulation of the cavernous nerves may represent an alternative to electrical nerve stimulation as a potential diagnostic tool during nerve-sparing radical prostatectomy.

Acknowledgments: This research was supported in part by an Idea Development Award from the Department of Defense Prostate Cancer Research Program, Grant #PC073709, and a Wachovia New Faculty Summer Research Grant from the Charlotte Research Institute.

IMAGE PROCESSING ALGORITHMS FOR USE IN OPTICAL COHERENCE TOMOGRAPHY OF THE CAVERNOUS NERVES IN THE PROSTATE

Shahab Chitchian[1], Michael Fiddy[1], and Nathaniel M. Fried[1,2]

[1] Department of Physics and Optical Science, University of North Carolina at Charlotte, NC
[2] Department of Urology, Johns Hopkins Medical Institutions, Baltimore, MD

Introduction: Preservation of the cavernous nerves during radical prostatectomy is critical in preserving sexual function after surgery. Optical coherence tomography (OCT) has recently been studied for potential use in nerve-sparing radical prostatectomy. However, improvements in OCT image quality are necessary prior to clinical use. Speckle noise occurs in OCT images when tissue components are smaller than the coherence length of the light source. Denoising attempts to remove this noise and retain signal regardless of the frequency content of the signal. Wavelet shrinkage denoising is performed by nonlinear soft thresholding in the wavelet transform domain. In this study, we compare the results of discrete wavelet transform (DWT) and dual-tree complex wavelet transform (CDWT) algorithms for wavelet shrinkage denoising in OCT images of the rat prostate.

Methods: The discrete wavelet transform provides the most compact representation, however, it has several limitations. It lacks the shift-invariance property, and in multiple dimensions it is inadequate for distinguishing orientations, which is important in image processing. The dual-tree complex wavelet transform overcomes these limitations, it is nearly shift invariant, and it is oriented in two dimensions. Image quality metrics were used to assess performance by measuring average contrast-to-noise ratio (CNR), average equivalent number of looks (ENL), and signal-to-noise ratio (SNR).

Results: The complex dual-tree wavelet transform performs better visually and by numerical metrics for wavelet denoising in the OCT images of cavernous nerves (Table 1).

Table 1. Image Quality Metrics

Image	CNR (dB)	ENL	SNR (dB)
Original	0.4135	2439	37.61
Denoised (DWT)	5.23	5342	55.10
Denoised (CDWT)	5.71	6469	54.76

Figure 1 on the right shows the OCT signals in a longitudinal scan of the prostate before and after denoising for comparison.

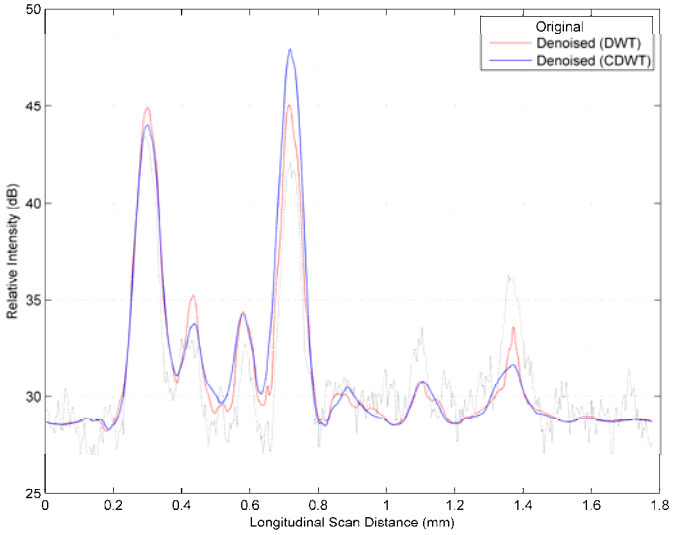

Conclusions: Image quality metrics of the cavernous nerves and signal-to-noise ratio were improved significantly using the complex wavelet denoising technique.

Acknowledgments: This work was supported in part by the Department of Energy, Grant #DE-FG02-06CH11460, an Idea Development Award from the Department of Defense Prostate Cancer Research Program, Grant #PC073709, and a Faculty Research Grant from UNC-Charlotte.

OPTICAL STIMULATION OF THE RAT CAVERNOUS NERVES

Gwen Lagoda, MS[1], Nathaniel Fried, PhD[2] and Arthur Burnett, MD[1]; [1]Johns Hopkins University, Baltimore, MD; [2]UNC Charlotte, Charlotte, NC
(Presented By: Gwen Lagoda)

Introduction: Improved diagnostic techniques are necessary for identification of the cavernous nerves (CN) during prostate cancer surgery and preservation of sexual function after surgery. This study explores the optimal laser parameters for stimulation of the CN based on intracavernosal pressure (ICP) responses.
Methods: Adult male rats (300-350 g) were used. Identification of CN's were first confirmed by electrical stimulation (4V, 60 s) followed by repeated laser stimulation with a thulium fiber laser. The laser pulse duration, laser spot diameter, and stimulation time were fixed at 2.5 ms, 1mm, and 60 s, respectively. Range of laser pulse energy (0.725 mJ – 7.5 mJ), pulse rate (5-20 Hz) and wavelength (1850-1880 nm) were tested at a variable optical penetration depth (300-600 μm) to approximate the nerve thickness. At the end of the study, electrical stimulation of the nerve was repeated to ensure viability after repeated laser stimulations. CNs were collected, processed and H&E-stained for histological examination.
Results: Optimal laser stimulation parameters were wavelengths of 1860-1870 nm, pulse energies greater than 2.7 mJ (0.35 J/cm^2), and a pulse rate of 10 Hz. ICP responses after laser stimulation were comparable to electrical stimulation (~ 50 mmHg). Histological examination showed no evidence of thermal damage to the nerves. However, as the pulse energy and/or pulse rate were increased, loss of nerve function was observed.
Conclusions: Laser nerve stimulation parameters can be optimized to evoke ICP responses similar in magnitude and duration to conventional electrical stimulation in a rat model. With further development, optical nerve stimulation may represent an intra-operative diagnostic technique for use in laparoscopic and robotic nerve sparing radical prostatectomy surgery.